

ATMOSPHERIC ANGULAR MOMENTUM FLUCTUATIONS IN GLOBAL
CIRCULATION MODELS DURING THE PERIOD 1979-1988

by

R. Hide^{1,3}

J. O. Dickey and S. L. Marcus¹

R. D. Rosen and D. A. Salstein²

¹ Space Geodetic Science and Applications Group
Jet Propulsion Laboratory,
California Institute of Technology,
4800 Oak Grove Drive
Pasadena, California 91109-8099, USA.
Tel: 818-354-3235; Fax: 818-393-6890

² Atmospheric and Environmental Research Inc. (AER)
840 Memorial Drive
Cambridge, Massachusetts 02139, USA.
Tel: 617-547-6207; Fax: 617-661-6479

³ Department of Physics (Atmospheric, Oceanic and Planetary
Physics)
University of Oxford
Clarendon Laboratory, Parks Road,
Oxford OX1 3PU England, UK.
Tel: 0-1865-272086; Fax: 0-1865-272924

Submitted to JGR-Atmospheres

ABSTRACT

Changes in major global dynamical phenomena in the Earth's atmosphere are manifested in the time series of atmospheric angular momentum (AAM), as determined directly from meteorological observations and indirectly from geodetic observations of small fluctuations in the rotation of the solid Earth that are proportional to length of day (LOD). AAM fluctuations are intimately linked with energetic processes throughout the whole atmosphere, and also with the stresses at the Earth's surface produced largely by turbulent momentum transport in the oceanic and continental boundary layers and by the action of normal pressure forces on orographic features. A stringent test of any numerical global circulation model (GCM) is therefore provided by a quantitative assessment of its ability to represent AAM fluctuations on all relevant time scales, ranging from months to several years. From monthly data provided by the Atmospheric Model Intercomparison Project (AMIP) of the World Climate Research Programme (WCRP), we have investigated seasonal and interannual fluctuations and the decadal mean in the axial component of AAM in 23 AMIP GCMs over the period 1979-1988. The decadal means are generally well simulated, with the model median value ($1.58 \times 10^{26} \text{ kg m}^2 \text{ s}^{-1}$) being only 3.5% larger than the observed mean and with 10 of the models being within 5% of the observed. The seasonal cycle is well reproduced, with the median amplitude of the models' seasonal standard deviations being only 2.4% larger than observed. Half the seasonal amplitudes lie within 15% of the observed and the median correlation found between the observed and model seasonal cycles is 0.95. The dominant seasonal error is an underestimation of AAM during northern hemisphere winter associated with errors in the position of subtropical jets. Less robust are the modeled interannual variations, though the median correlation of 0.61 between model simulation and observed AAM is statistically significant. The two El Niño-Southern Oscillation (ENSO) events that occurred during the AMIP decade 1979-1988 have the expected positive AAM anomalies though the AAM signature of the 1982-1983 event tends to be underestimated, and that of the 1986-1987 event overestimated.

1. INTRODUCTION

The Earth's atmosphere super-rotates relative to the underlying planet such that, if transferred to the solid Earth below, the angular momentum associated with this super-rotation would reduce the length of the day (LOD) by around 3 milliseconds. Geodetic observations going back several decades reveal irregular LOD fluctuations of up to about 1 ms on interannual, seasonal and intraseasonal time scales (see Fig. 1), and detailed studies using modern meteorological and geodetic data have established that

Figure 1 near here

these fluctuations are largely of meteorological origin (for reviews, see Hide and Dickey, 1991; Rosen, 1993; Dickey 1993; Eubanks, 1993 and references (herein). Fluctuations in the equatorial components of atmospheric angular momentum (see Appendix A) are associated with non-axisymmetric features of the global atmospheric circulation and make a substantial contribution to polar motion (the observed wobble of the rotation axis of the solid Earth with respect to geographical coordinates) on sub-decadal time scales. On decadal and longer time scales [Fig. 1 (b)], the dominant forcing is due to non-meteorological agencies, inducing angular momentum exchange between Earth's liquid metallic core and the overlying solid mantle and "spin-orbit" coupling between Earth and Moon largely associated with tidal friction in the oceans. The angular momentum of the oceans is not well determined owing to the paucity of data; however, fluctuations in magnitude in their axial component are no more than 10% of those of the axial component of AAM (hereafter used as an abbreviation for the axial component of atmospheric angular momentum) with which this paper is concerned.

The task of improving the performance of numerical models of the atmosphere by identifying and correcting weaknesses in their formulation requires systematic methods for testing model performance. The inclusion of diagnostics based on analyses and

forecasts of AAM offers several advantages. The most obvious is the unique opportunity it provides, in principle at least, for comparing on a clear-cut physical basis the output of a global quantity from the models with observations that are completely independent of meteorological data, namely those of short-term fluctuations in the LOD. The axial torques at the Earth's surface responsible for meteorologically-induced fluctuations in the Earth's rotation are produced by (a) tangential stresses in turbulent boundary layers and (b) normal (pressure) stresses acting on irregular topography. These stresses are transmitted directly to the solid Earth over continental regions and indirectly over the oceans.

Secondly, considerations of AAM fluctuations bear directly on fundamental aspects of the energetic of the global atmospheric circulation and cannot be separated from them. In the absence of energy sources, the atmosphere would rotate with the solid Earth like a rigid body (i.e., no winds), for this would be a state of minimum kinetic energy of the whole system for a given total angular momentum. Differential solar heating produces atmospheric winds, the kinetic energy of which derives from the available potential energy of the atmosphere (associated with gravity acting on the density field maintained by the heating) through the action of vertical motions. Angular momentum is thereby redistributed without any change occurring in the total amount in the whole system (since solar heating produces no net torque) but with an increase in the total kinetic energy. A substantial contribution to this energy is associated with 'super-rotation' of the atmosphere at an average azimuthal wind speed U (say) of about 7 ms^{-1} , namely $\frac{1}{2}MU^2$ if M is the total mass of the atmosphere. Observed fluctuations in AAM amount to a considerable fraction of the mean MUR in magnitude (where R is the mean radius of the solid Earth). Concomitant fluctuations in the kinetic energy associated with the super-rotation amount to a considerable fraction of the mean $\frac{1}{2}MU^2$. By energy conservation arguments, these can only be produced by dynamical processes involving nonlinear interactions between the zonal wind field, the non-zonal wind field, and the

field of available potential energy in the atmosphere. Successful models of the global circulation of the atmosphere must of course represent these interactions correctly. (For further details see Bell *et al.*, 1991.)

Thanks to the First GARP Global Experiment (FGGE) of the Global Atmospheric Research Programme (GARP) it became possible to obtain useful daily determinations of the total AAM for comparison with geodetic data on LOD variations [Hide *et al.*, 1980]. Manifold subsequent developments following this early work include practical arrangements for producing and disseminating routine daily or more frequent determinations not only of the axial component of the AAM vector but also of the equatorial components [Barnes *et al.*, 1983; Salstein *et al.*, 1993]. These determinations (see Appendix A, equations A7 to A9) are now made from analysis (and in some cases also from forecast) fields by several meteorological centers, namely the European Centre for Medium-Range Weather Forecasts (ECMWF), Japanese Meteorological Agency (JMA), United Kingdom Meteorological Office (UKMO), and United States National Meteorological Center (NMC, recently renamed National Centers for Environmental Prediction, NCEP). Plans are now in hand at some centers for producing routine determinations of surface torques, which will supplement the AAM data and facilitate diagnostic studies.

The ambitious Atmospheric Model Intercomparison Project (AMIP) of the World Climate Research Programme (WCRP) is one of the main activities initiated by the WCRP's Working Group on Numerical Experimentation (WGNE) in its efforts to refine atmospheric models and improve their ability to produce useful forecasts of changes in weather and climate [Gates, 1992]. Thirty atmospheric modeling groups cooperate unselfishly in AMIP, together with more than twenty groups engaged in diagnostics subprojects of AMIP concerned with the thorough testing of models by means of quantitative intercomparisons of their ability to reproduce various aspects of the behavior of the atmosphere. Our efforts in the atmospheric angular momentum diagnostics

subproject of AMIP bear directly on the extent to which zonal winds and the exchange of angular momentum between the atmosphere and the underlying planet are represented correctly by the models being tested.

Specific dynamical phenomena produce strong signatures in observed AAM fluctuations and the study of the angular momentum balance of the Earth-atmosphere-ocean system is relevant to many climate dynamics issues. Earth relation variations provide a unique and truly global measure of changes in the atmosphere, oceans, and cryosphere, on time scales ranging from days to centuries. The variation of AAM has now been convincingly linked to sub-decadal changes in the length-of-day down to time scales of about a week [Dickey *et al.*, 1992]. The axial component of the total AAM shows a characteristic seasonal variation and pronounced 'broad-band' intraseasonal fluctuations [Figs. 1(d) and (c)]. Oscillations on intraseasonal time scales, including those related to the Madden-Julian oscillation, have been shown to involve AAM changes propagating within the tropics [Anderson and Rosen, 1983], with contributions from orographically forced oscillations in the extratropics [Dickey *et al.*, 1991 and Marcus *et al.*, 1994]. The accurate characterization of the seasonal AAM cycle involves the whole atmosphere from 1000 to 1 mb, with stratospheric winds making a significant contribution [Rosen and Salstein, 1985; and Dickey *et al.*, 1994].

LOD and AAM also exhibit interannual variations, on quasi-biennial and quasi-quadrennial time scales [Chao, 1984, 1988, 1989; Dickey *et al.*, 1992, 1994; Eubanks *et al.*, 1986; Jordani *et al.*, 1995; and Salstein and Rosen, 1986-see Fig. 1 (c)]. Well-correlated with ENSO events, these are associated with large-scale zonal-wind anomalies which appear to propagate from tropical to extra-tropical regions [Dickey *et al.*, 1992; Salstein *et al.*, 1993]. Teleconnections between different latitude bands have been discovered in AAM data on these time scales, providing insights into the global structure of interannual climate variations [Dickey *et al.*, 1992; Salstein *et al.*, 1993; and Marcus and Dickey, 1994]. Indeed, much progress has been made during the past twenty years with the

investigation of AAM fluctuations on sub-decadal time scales. important new results can be expected from future studies, including numerical simulations of AAM fluctuations on decadal and longer time scales. Such studies, in addition to their intrinsic interest in meteorology and oceanography, will indirectly facilitate investigations of angular momentum exchange between the Earth's liquid metallic outer core and overlying mantle and other non-meteorological processes which, though evidently relatively unimportant on sub-decadal time scales in the excitation of irregular fluctuations in the Earth's rotation, play dominant roles on longer time scales.

The data used and methodology employed in our study are outlined in Section 2, setting the scene for the axial AAM intercomparisons of decadal means and on seasonal and interannual time scales, presented and summarized in Section 3 and 4. In the future work it will be important to investigate the extent to which atmospheric models can reproduce fluctuations in the equatorial components of atmospheric angular momentum. These excite measurable movements in the Earth's pole of rotation on sub-decadal time scales, including a Chandlerian free wobble with a period of 14 months (see Appendix A).

2. DATA AND METHODOLOGY

a. Observed values of angular momentum

The most complete series of AAM and zonal wind fields generally available for the AMIP decade (1979-1988) are those produced operationally by the NMC. (comparisons of the NMC AAM series with one from the ECMWF [Rosen *et al.*, 1987; Rosen, 1993; Dickey *et al.*, 1993] indicate that the differences between the two series are so small that we can confidently use either for validating the AMIP model results. Up to twice-daily values of zonal-mean zonal wind [u] from the NMC have been archived on a 2.5° latitude grid at standard pressure levels between 1000 and 50 mb. We created monthly mean fields of [u] by averaging all data available within each calendar month

during 1979-1988. These fields were then used to create a monthly series of the relative angular momentum (M^w) of the atmosphere about the polar axis by applying equation (A 13) and evaluating

$$M^w = 2\pi \bar{R}^3 g^{-1} \int_{50}^{1000} \int_{-\pi/2}^{\pi/2} [u] \cos^2 \phi \, d\phi \, dp. \quad (2.1)$$

In addition to the global M^w values, we also computed the relative angular momentum of the atmosphere in each of 46 equal-area belts (m_b^w) over the globe to help isolate regional sources of model errors in (m_b^w). As explained by Rosen and Salstein [1983], the number of belts is dictated by the 2.5° latitude resolution of the NMC analyses and the constraint that all belts should have the same area as that between the equator and 2.5° N. The latitudinal boundaries of the resulting 46 belts are listed by Rosen and Salstein [1983]. Within each belt, m_b^w is given by

$$m_b^w = 2\pi \bar{R}^3 g^{-1} \int_b \int_{50}^{1000} [u] \cos^2 \phi \, d\phi \, dp, \quad (2.2)$$

where ϕ runs between the southern and northern boundaries of belt b . In evaluating this expression numerically, care was taken to ensure that $\sum_{46 \text{ belts}} m_b^w = M^w$ is satisfied each month. Although the creation of m_b^w values precludes consideration of variability within a vertical column, the results of Rosen and Salstein [1983] suggest that such variability is often more coherent than that in the meridional direction. To maintain a manageably sized regions] data set, therefore, we feel it sufficient to limit the bulk of our intra-global analyses here to m_b^w .

b. Model values of angular momentum

Monthly mean values of $[u]$ were available from 29 GCMs at the time of writing as part of the standard output archived by AMIP [Gates, 1992]. All but 5 of the GCMs

include pressure levels up to 50 mb, and these 5 models were eliminated from further consideration to maintain consistency with the depth of the atmosphere in the NMC observations.¹ By the same token, levels above 50 mb that may have been available for an AMIP model are disregarded here. The model values of $[u]$ are given on two-dimensional latitude-pressure grids whose resolutions vary from model to model. To simplify computations, however, we interpolated all model output to the same 2.5° latitude grid as the NMC observations, although we retained each model's archived distribution of pressure levels when computing M^w and m_b^w .

Model results shown here are identified by the acronyms defined by Gates [1992], as updated by Phillips [1994] (see Table 1).² The latter report summarizes the major characteristics of each AMIP model, and no attempt to reproduce that information in any detail is made here. It is clear from this documentation, however, that the set of AMIP models is heterogeneous, embodying a wide range of choices in resolution and physical parameterizations; hence an assumption that the relatively small sample of M^w values available to us is drawn from a statistically normal population is not justified. We, therefore, avoid using the mean and standard deviation as measures of central tendency and spread, respectively, of the distribution of model M^w values. Instead, we use the median and the inter-quartile range (IQR) described by Lanzante [1996] for these statistics. The IQR is simply the difference defined by the upper quartile minus the lower quartile of values in the distribution; i.e., it measures the distance spanned by the middle half of the distribution. An advantage of the IQR is that it is relatively resistant to the presence of large outliers, unlike the standard deviation. For a Gaussian distribution, however, the two statistics are related: in this case the IQR is 1.349 times the standard deviation [Lanzante, 1996].

¹Output from GISS was also disregarded, because of its unusual vertical distribution

²An exception is the SUNYA/NCAR model, which we abbreviate as SNG.

c. Temporal decomposition

Rosen *et al.* [1991b] and Hide and Dickey [1991] illustrate that the temporal variability in the Earth-atmosphere system can be usefully separated into three frequency bands: intraseasonal, seasonal, and interannual. A decomposition for LOD, which also experiences substantial decadal variability due to core-mantle interaction, is shown in Fig. 1. The seasonal cycle is by far the dominant sub-decadal signal, being -1 ms in peak to peak amplitude and typically explaining, more than 75% of the variance in the total series [see Fig. 1(a)]. Hence, our inability to consider intraseasonal variations in M^w here [Fig. 1(e)] because of the monthly mean resolution of the AMIP' standard output is not overly limiting. To define the seasonal component of each of the model and observed M^w series, we first removed their decadal means, i.e., the average of the 120 monthly values for 1979-1988, and then averaged the 10 values for each calendar month. An interannual component, which is considerably smaller than the annual signature, is formed by averaging the monthly values in each of the 40 "seasons" during the decade, beginning with January-March 1979, and subtracting from this series the decadal mean seasonal cycle. Although this "interannual" component includes some higher (non-seasonal) frequency variability, we will see that the bulk of its variance is from time scales longer than a year. Hence the term "interannual" is appropriate for this component.

in the next section, we compare the decadal mean, seasonal, and interannual components of the 23 model M^w series with the. observed components obtained from the NMC analyses. As noted above, the accuracy of the NMC analyses is not a significant issue here; the differences found among the. model M^w series are typically much larger than the uncertainty in the observed series.

3. RESULTS

Time series of M^w for each of the 23 AMIP models are. shown in Figure 2 (solid lines)

2 nc Figure 2 near here

and are contrasted with M^w determined from the operational NMC analysis (dashed lines) and that inferred from geodetic data (dotted lines). The observed AAM and LOD track each other with a high degree of fidelity, although the amplitude of the annual and interannual components of the observed AAM are somewhat under-estimated relative to the LOD, partly because of neglect of the atmosphere above 50mb [Rosen and Salstein, 1985 and Dickey *et al.*, 1994]. The overall agreement between the simulated and observed results is fairly good, but significant biases are found in some cases, with several models showing values which are consistently higher or lower than the observed AAM (note that LOD cannot be used to infer the time-averaged value of AAM, since its definition includes an arbitrary reference level). The dominance of the seasonal cycle is evident in all data sets, with amplitudes significantly less than the observed value visible for several of the models, while greater amplitudes are obtained for others. On interannual time scales, the large signature of the 1982-83 ENSO is clearly seen in both the AAM and LOD time series. This signal is well-captured by several of the models, but not by others. These broad findings are evident in the following detailed intercomparisons of the decadal mean AAM and AAM fluctuations on seasonal and interannual time scales as given by the AMIP models and by operational NMC analyses

a. Decadal mean

The global atmosphere's super-rotation is its most striking dynamic, long-term feature. During the AMIP decade 1979-1988, the observed mean value is $1.51 \times 10^{26} \text{ kg m}^2 \text{ s}^{-1}$ which, if transferred to the underlying solid Earth would, if the solid Earth were perfectly rigid, reduce the length of the day by 2.5 ms (see equations (A7), (A9), (A10) and (A11)). Values yielded by each of the AMIP models are plotted in Figure 3, along with the median and IQR of the model values. The model median M^w is

Figure 3 near here

only 3.5% larger than the observed value with 10 of the 23 model] values within $\pm 5\%$ of the observed. More significant departures from the observed value are found in other models, 5 of which give values differing by more than 15% from the observed. Included in this group of poorer results is that from the NMC; because versions of the NMC model were at the heart of the four-dimensional data assimilation system that created the validation values used here, the NMC model's lack of success in Figures 2 and 3 suggests that observations are indeed capable of modifying a model's initial guess field in modern data assimilation schemes.

Figures 2 and 3 suggest that biases in GCM simulations of the zonal wind field are not uniform, and the identification of the causes of the observed discrepancies may not be straightforward. The difficulties involved are evident from Figure 4, in which the

Figure 4 near here

decadal-mean observed $[u]$ and the errors in $[u]$ are shown for those models that yield, respectively, the two largest and the two smallest values of M^w in Figure 3. Remarkably, the meridional distribution of the bias in $[u]$ shows wide variations, even within each class of model errors in M^w . Thus, the main source of the large value for the decadal mean of M^w seen in the UCLA model is excess values of $[M]$ above 200 mb from 60°N to 60°S , whereas the erroneously large NCAR value of M^w arises primarily from $[u]$ errors below 200 mb. The low value of the mean M^w seen in the NMC model results arises from systematically low values of $[u]$ throughout the tropics, particularly in the upper troposphere and lower stratosphere, whereas the very low value of the mean M^w from the DNM results has its source in extratropical regions, with the tropics contributing a positive but smaller bias.

For comparison, Figure 5 gives the $[u]$ -bias field for the GLA model, whose

Figure 5 near here

decadal-mean M^w lies closest to that observed for 1979-1988. It appears that success in reproducing the global mean value of M^w need not imply similar success with the decadal-mean $[u]$ field, for the magnitude of the $[u]$ biases evident in Figure 5 is of the same order as those shown in Figure 4 for the outlier M^w simulations. Evidently, for the GLA model at least, the good performance for decadal-mean M^w arises from the cancellation among regional biases in $[u]$ of opposite sign, biases which in many locations are comparable to the observed value of $[u]$ there (cf. Figure 4a). The (area-weighted) mean absolute error in $[u]$ for the GLA field in Figure 5 is 2.3 ms^{-1} . At 1.9 ms^{-1} (IQR = $2.3 - 1.7 \text{ ms}^{-1}$), typical values of this statistic are smaller than the observed mean absolute value of $[u]$ in Figure 4a, 8.5 ms^{-1} , but not by so much that we can be sanguine about this aspect of the performance of the models.

Despite the differences shown in Figure 4 for $[u]$ among an outlier subset of AMIP models, it remains of interest to quantify the similarity in model biases among the general population of AMIP models. To this end, we have performed an empirical orthogonal function (EOF) analysis of the biases present in the set of m_b^w values in the 46 belts for the 23 models. Three significant modes of common variability in the belt momentum error distribution emerge (Figure 6) which together explain more than 80% of

Figure 6 near here

the variance in the full ensemble of m_b^w biases. Mode 1, involving errors primarily in northern and southern mid-to-high latitudes with a tendency for smaller, compensating errors in the subtropics, is notable in that the weights for 19 of the models in its principal component are of the same sign. Recognizing that errors for a particular mode are often spread across all three modes, the commonality of behavior expressed by mode 1's principal component nevertheless suggests the existence of a shared, underlying difficulty

in modeling the climatological, regional distribution of angular momentum. Mode 2 reveals a pattern in which biases in the tropics and in northern midlatitudes are in opposition, and mode 3 emphasizes behavior in southern extratropics.

b. Seasonal cycle

The seasonal cycle in AAM derives from the asymmetry in the land-ocean distributions of the northern and southern hemispheres and the resulting difference in the seasonality of the two hemispheres' subtropical jets [Rosen *et al.* 1991b]. Because the seasonal cycle represents the largest mode of variability in the AAM time series, it is important that GCMs be able to replicate this signal well. It is encouraging, therefore, to see in Figure 7 that the AMIP models do tend to reproduce the behavior observed in the

Figure 7 near here

climatological monthly mean progression of M^w values. It is worth noting, however, that the models also exhibit a general tendency to underestimate the maximum values observed in December--February. Indeed, in some models this deficiency is quite pronounced, leading to seasonal cycles with distinct maxima around April and November instead of the observed single broad maximum across December through April.

The degree to which the models share common problems in reproducing the observed shape of the seasonal cycle in M^w is revealed by an EOF analysis of the models' composite monthly errors (Figure 8). The tendency of the models to underestimate M^w

Figure 8 near here

during northern winter is apparent in both of the first two modes of this analysis by the preponderance of positive model weights multiplying negative anomalies in the modes' time series then. The first mode in Figure 8 captures errors in the models' estimates of the annual component of M^w , whereas the second mode captures errors in their semiannual

component. (The semiannual component of M^w is normally observed to peak in early May, and its amplitude is about 80% of that of the annual component, which peaks in early February; Rosen, 1993). The general shortcoming of the models in December-February appears to project onto a proclivity towards underestimating the annual, while overestimating the semiannual, component of the observed seasonality in M^w .

Figure 9 displays a measure of the amplitude of the seasonal cycle, namely the

Figure 9 near here

standard deviation (σ_s) of the twelve composite calendar-month means of M^w , for each AMIP model and the observed series. The median σ_s value is only some 2.4% larger than the observed σ_s , with nearly half of the model values lying within about 15% of the observed. Nevertheless, notable outliers also exist in Figure 9, so that the range in values for σ_s exceeds a factor of two. There does not appear to be any relationship between errors in a model's seasonal cycle and in its decadal-mean bias, with high values of σ_s being equally likely to be associated with either high or low values of (decadal-mean M^w in Figure 3 (and similarly for low values of σ_s). Also shown in Figure 9 is the correlation coefficient (r_s) between each model's series of composite monthly M^w values and the observed series. In conjunction with σ_s , the r_s statistic helps provide a more complete analysis of the fidelity of a model's simulation. Not surprisingly in light of Figure 7, r_s is generally quite large (median = 0.95; IQR = 0.97- 0.92).

Although the bulk of the observed seasonal variability in m_b^w occurs in

Figure 10 near here

connection with the subtropical jets of each hemisphere (Figure 10a), this need not imply that the errors present in Figure 9 originate mostly there. Therefore, to isolate regionally the source of seasonal model errors in M^w , we have calculated for each model: (1) the variance in the difference between the composite monthly mean values of its belt series

m_b^w and the observed m_b^w values, and (2) the covariance between these seasonal errors in the model belt values and the seasonal errors in global M^w , normalized by (the variance in the latter. Because the sum of the covariance in (2) over all 46 belts is equal to the variance in a model's seasonal errors in global M^w , the sum of the 46 values of (2) for a particular model is unity. Hence, (2) provides a convenient measure for quantifying the contribution made by seasonal errors in various regions to the global error. as was done by Rosen *et al.* [1991a] in connection with medium-range forecast model errors.

Errors in the models' simulations of m_b^w seasonal cycles are less spatial]]' focused than is the profile of the observed m_b^w variance in Figure 10a. Indeed, a plot of (1) as a function of latitude for the 23 models is too noisy to be useful, so Figure 10b attempts to summarize this result by presenting a profile of the median in each belt of all the models' seasonal belt error variances, along with the IQR of these 23 numbers. The large values of the IQR in the figure, especially in the extratropics s, attest to the strikingly wide range of model behavior. (Note that the median values plotted in Figure 10 are determined individually for each belt; the profile. does not represent the behavior of a single, "median" model.) The largest model errors in simulating the observed seasonal cycles in m_b^w tend to flank both sides of the two maxima in Figure 10a, suggesting that errors in positioning the subtropical jets properly are a factor'. On the other hand, the amplitude of the largest median errors in Figure 10b is considerably smaller than [hat of the observed variance peaks in Figure 10a, suggesting that the models do a credible job in reproducing the seasonal change in the *strength* of the subtropical jets.

The fractional covariance between seasonal belt and global momentum errors plotted in Figure 10c indicates that, on average, the model errors that contribute most to failures in reproducing the observed seasonal cycle. in M^w originate in the equator most pair of peaks in Figure 10b, near 20°N and 15°S. The large local errors in northern midlatitudes shown in Figure 10b tend not to be so important for the globally-integrated error. Note again, however, the very large spread in model behavior outside the tropics

depicted by the IQR values; for a number of models, errors poleward of the observed positions of the subtropical jets are indeed a major reason for problems with simulating the seasonality in M^w .

c. Interannual variations

The AMIP decade encompassed two ENSO events, those of 1982-1983 and 1986-1987. The former is possibly the strongest such event on record, and the notable positive anomaly in AAM and LOD associated with it led to a resurgence of interest in low-frequency variations in the planetary angular momentum budget. (For recent results and references see Ponte *et al.*, 1994, and Dickey *et al.*, 1994.) The signature of the two ENSO events during 1979-1988 AMIP period is apparent in the observed interannual M^w anomaly series in Figure 11 as a sharp peak in early 1983 and a broader, less intense

Figure 11 near here

maximum from late 1986 through 1987. On average, the AMIP models reproduce the observed interannual anomaly series fairly well, though less successfully than in the case of the seasonal cycle (Figure 7). It is noteworthy that the models, as a group, tend to underestimate the amplitude of the 1982-1983 ENSO signal in AAM but overestimate the 1986-1987 signal. The models also miss the intensity of the negative anomaly observed in 1984, although they do capture the rate of decline in M^w during 1983 fairly well. Notably, though, the models miss even the sign of the anomaly observed during mid-1980 through mid-1981, which according to the NMC observations results mainly from positive wind anomalies in the southern hemisphere tropics (not shown).

Figure 12 gives the interannual standard deviation (σ_1) for each mode

Figure 12 near here

separately, along with the correlation coefficient (r) between each model's time series of 40 seasonal anomalies and the observed. The median value of σ_I is quite close to the observed, and, as in the case of the seasonal cycle, almost half of the model σ_I values lie within about 15% of the observed, although in the interannual case there is a notable skewness in the distribution toward low values. No relationship between individual σ_I and σ_S values is evident in the data; the performance of each model on one time scale seems to be independent of its performance on the other (see Table 1). A striking

Table 1 near here

difference between overall model performances on seasonal and interannual time scales is that r_I is notably smaller than r_S . The median of r_I is 0.61 with 0.66-0.49 as the corresponding IQR value. On the basis of calculations of the autocorrelation present in the observed and modeled anomaly series, we estimate that in each series the number of degrees of freedom is about 12, implying that a value of r_I greater than about 0.5 is to be regarded as being statistically significant. Sixteen of the models (nearly 70%) exceed this criterion.

Calculations similar to those reported in Figure 10 for the seasonal cycle in m_b^w have also been performed for interannual variability in m_b^w , and these are reproduced in Figure 13. The meridional profile of median model errors in the m_b^w interannual

Figure 13 near here

component tends to be spatially correlated with the profile of the observed interannual variance in m_b^w (Figure 13a). Unlike the case for the seasonal cycle, local errors in the interannual m_b^w component are typically of the same order as the observed signals across the entire profile. Indeed, interannual errors in m_b^w are not much smaller than seasonal errors in m_b , despite the disparity in the amplitude observed for the two time scales. According to Figure 13b, errors in m_b^w within 200 of the equator account for most of the

interannual errors in M^w . In light of the relatively small values of IQR also plotted in Figure 13b, this result is rather robust across the suite of 23 AMIP models.

4. DISCUSSION AND SUMMARY OF RESULTS

here, we have presented results of a study comparing atmospheric angular momentum (AAM) simulations by a variety of AMIP models (Table 1) with the NMC observed values and those inferred from geodetic data. Results from 23 AMIP model runs were considered on three distinct time scales: decadal mean, the seasonal cycle, and interannual variation. Of the 23 models (Table 1), 4 scored well (being within $\pm 15\%$ of that observed) on all three time scales, 10 on two out of three, 6 on one of the three and 3 performed poorly on all three time scales. It should be stressed that the GCM results presented here represent "snapshots" (each year 1990s) of model evolution that is ongoing at the participating centers. For example., a new gravity-wave drag parameterization scheme has recently been developed at UCLA (Kim and Arakawa 1995), which shows considerable promise for reducing the westerly bias present in the UCLA GCM, in conjunction with an envelope orography (Kim, 1996).

The decadal mean values of AAM were generally well-simulated, with the model median value ($1.58 \times 10^{26} \text{ kg m}^2 \text{ s}^{-1}$) being only 3.5% larger than the observed. Ten of the 23 models produced values that are within 5% of the observed mean; however, 8 of the 23 models are more than 15% away from the observed (Table 1). Examination of the decadal-mean [u] bias with respect to observed winds as a function of latitude and height indicates that contributing errors may be very different in models that show the same characteristic global anomaly (Fig. 4). Furthermore, good agreement with the observed decadal mean cannot be taken to infer similar agreement with the observed [u] fields (Fig. 5), as cancellation among regional differences may combine to produce a low global bias. An EOF analysis performed on angular momentum values in the 46 belts for the 23 models produced 3 dominant modes explaining 87% of the variance. Both Mode 1

(involving errors in the northern and southern mid-to-high latitudes with smaller partially canceling errors in the subtropics) and Mode 2 (bias in the Tropics with compensating bias in the northern midlatitudes) are common to the majority of the models, indicating shared problems in modeling the latitudinal distribution of mean angular momentum.

The seasonal cycle results from asymmetry of the land-ocean distribution of the northern and southern hemispheres, and is generally well-simulated in the AM]]' models. The median seasonal standard deviation (σ_s) value is 2.4% larger than observed, with 10 of the models being within 15% of the observed amplitude (Fig. 9 and Table 1). Four of the five models with decadal means that do not lie within 15% of the observed have seasonal variations that do not lie within 15% of the observed value, suggesting that there may be some linkage between poor model performance on decadal means and seasonal time scales. The correlation between observed and model seasonal cycles is quite high, with a median value of $r_s = 0.95$ (IQR = 0.97-0.92). An EOF analysis provides insight into common seasonal errors; the first mode shows a tendency for most models to underestimate the annual cycle, while the second mode largely reflects overestimates of the semi-annual cycle (Fig. 8), both consistent with the models' tendency to underestimate global AAM during northern hemisphere winter. The observed seasonal cycle in AAM is dominated by contributions from the subtropical Jets from each hemisphere (Fig. 10), whose strength is generally well reproduced by the models. The largest regional model errors, whose seasonal variance is about an order of magnitude smaller than the observed variance (Fig. 10), tend to border on both sides of the two hemispheric maxima, indicating that errors in positioning the subtropical jets are an issue. Further, examination of the fractional covariance between the regional and global momentum errors (Fig. 10) indicates that most of the seasonal M^w errors originate equatorward of the subtropical jets.

The models' interannual AAM variability is fairly realistic, with the median value of σ_I being quite close to the observed value and ten of the model σ_I values lying within

15% of the observed. Although less robust than the seasonal cycle, the correlation between the observed and model interannual series has a statistically significant median value of 0.61. The two ENSO events during the AMIP decade are clearly evident; however, accurate simulation of intensities of the AAM signatures of individual episodes is generally lacking, as the 1982-1983 event is underestimated and the 1986-87 event is overestimated by the model consensus (Fig. 11). Examination of the latitudinal error covariance structure shows that errors within 20° of the equator account for most of the interannual mismodeling of M^w (Fig. 13b). No relationship is evident between errors on interannual and seasonal time scales in a given model (see Table 1).

The principal objective of AMIP is to identify deficiencies in numerical models so that they can be removed. Except near the equator, the thermal wind relationship based on quasi-geostrophic balance in the horizontal and hydrostatic balance in the vertical relates the vertical rate of change of horizontal wind to the local horizontal gradient of potential density, which depends on temperature, pressure, and moisture content. In using this relationship to obtain a good leading approximation to the wind itself at a general point in the atmosphere, there is a horizontal function of integration which can be evaluated from the surface winds. It follows that any model that satisfactorily represents both (a) surface winds, and (b) horizontal variations of temperature and moisture content should score well on the angular momentum assessment carried out in this paper, and conversely. It is possible, of course, that models that represent angular momentum fluctuations well might, owing to compensating errors, be doing so for the wrong reasons. For example, many of the models participating in the AMIP campaign show cold biases in both the tropics and extratropics [Fiorino, 1995]; the matching sign of these temperature biases serve to minimize errors in the meridional temperature gradient, which in turn helps many of the models to achieve realistic values for the decadal mean AAM.

In any event, it is obvious that any modeling groups exploiting the results presented in this paper should in the first instance examine those features of the model

that determine the pattern of surface winds and the distribution of temperature and moisture within the atmosphere. Of particular importance will be parameterization schemes for representing oceanic and continental boundary layers, mechanical interactions of the atmosphere with orography, including drag due to the excitation of gravity waves, and the role of moist convection and radiative processes in the atmosphere, where the presence of clouds introduces serious complications now being studied intensively in various meteorologic] research centers.

These remarks might facilitate the use of atmospheric angular momentum "skill scores" in the important and by no means straightforward task of identifying deficiencies in parameterization schemes used in numerical models, with a view to improving the schemes. Much careful work will be needed, however, for a cursory inspection of skill scores reveals no striking correlations with any of the manifold characteristics (see above paragraphs) of the various models used by groups participating in AMIP (cf. Phillips, 1994). In fact, no common characteristics are shared by the four models that are successful on all three time scales. The continuing Atmospheric Model Intercomparison Project will provide opportunities to pursue the necessary investigations.

Acknowledgments. We thank the members of the modeling groups who sent results to the Atmospheric Model Intercomparison Project (AMIP) of the World Climate Research Programme (WCRP) and we especially wish to thank W. L. Gates and his colleagues at the Lawrence Livermore Laboratory, who coordinated the AMIP effort. We acknowledge interesting discussions with C. R. Mechoso, K. Sperber, and G. H. White. The work of J. O. Dickey and S. L. Marcus was carried out at the Jet Propulsion Laboratory, California Institute of Technology, under contract with the National Aeronautics and Space Administration. Programming assistance at AFER was provided by P. Nelson. The work of R. D. Rosen and D. A. Salstein was supported in part by the National Science

March 18, 1996

Foundation Climate Dynamics Program under grant ATM-9223 164, and NASA's Mission to Planet Earth Program under Contract NAS5-32861 and Grant NAC;W-7615.

APPENDIX A: ATMOSPHERIC EXCITATION OF
EARTH'S ROTATION VARIATIONS

The absolute angular momentum of the atmosphere, a three-dimensional vector $M_i = M_i(t)$ (where t denotes time), can be written as the sum of two terms

$$M_i \equiv M_i^P + M_i^W \quad (A1)$$

where
$$M_i^P \equiv \iiint \rho \epsilon_{ijk} x_j \epsilon_{klm} \omega_l x_m d\tau \quad (A2a)$$

and
$$M_i^W \equiv \iiint \rho \epsilon_{ijk} x_j u_k d\tau, \quad (A2b)$$

respectively the 'matter' (or pressure) and the 'wind' contributions to M_i . here $\rho(x_i, t)$ and $u_k(x_i, t)$ denote the mass density and wind velocity respectively at a general point, x_i , $i = 1, 2, 3$ within the atmosphere, and $d\tau$ is a volume element of the atmosphere, over the whole of which the volume integral is taken. The usual summation convention is used for repeated suffixes, and ϵ_{ijk} is the alternating tensor with values 0 or ± 1 . The frame of reference used has its origin at the center of mass of the whole Earth (solid inner core, liquid outer core, 'solid Earth', hydrosphere, atmosphere) and is aligned with the principal axes of inertia of the 'solid Earth' (mantle, crust and cryosphere). With respect to an inertial frame, the rotation of the solid Earth has angular velocity $\omega_i(t)$, $i = 1, 2, 3$.

All components of M_i vary with time as a consequence of dynamical interactions between the atmosphere and the underlying planet, which produce measurable fluctuations in ω_i . It is customary to write

$$\omega_i(t) \equiv (\omega_1(t), \omega_2(t), \omega_3(t)) \equiv \Omega (m_1(t), m_2(t), 1 + m_3(t)), \quad (A3)$$

where $\Omega = 7.292115 \times 10^{-5}$ radians per second is the mean angular speed of sidereal rotation of the solid Earth in recent times. Over time scales that are short compared with

those of geological processes, the magnitudes of the dimensionless quantities $m_1(\sim)$, $m_2(t)$ and $m_3(t)$ are all very much less than unity, so that for the purpose of determining M , from meteorological data using equations (A2), it is sufficient to set $m_i = 0$, so that $\omega_i = (0, 0, \Omega)$.

The non-zero meteorological contributions to $m_i(t)$ are, of course, important in the study of fluctuations in the Earth's rotation. If L_i ($i = 1, 2, 3$), is the net torque acting on the Earth's atmosphere then

$$L_i = (dM_i/dt) + \epsilon_{ijk} \omega_j M_k, \quad (A4)$$

where dM_i/dt and \dot{M}_i are the time rates of change M_i in an inertial frame and in the rotating frame respectively. When $\omega_i = (0, 0, \Omega)$ we have

$$L_1 = \dot{M}_1 - \Omega M_2, L_2 = \dot{M}_2 + \Omega M_1, L_3 = \dot{M}_3 \quad (A5)$$

It is well known that L_i cannot be determined as accurately as M , from surface drag and pressure force determinations, owing to limited measurements, parameterization difficulties, and the high degree of cancellation involved. But it can be determined indirectly with useful accuracy from mass and wind observations at α levels within the atmosphere by using the expressions given by equations (A4) [White, 1991 and 1993; Salstein and Rosen, 1994]. Through the action of L_i , angular momentum is exchanged back and forth between the atmosphere and the underlying planet, the surface of which is subjected by the atmosphere to an applied torque equal to $-L_i$. Most of the angular momentum exchanged, which in magnitude can be a considerable fraction of that of M , goes into the massive solid Earth, whose moment of inertia is some 10^6 times that of the atmosphere. This produces (a) tiny but measurable changes in the length of the day

$$\Lambda(t) = \Lambda_0 / (1 + m_3(t)), \text{ where } \Lambda_0 \equiv 2\pi / \Omega, \quad (\text{A6a})$$

as well as (b) movements of the poles of the instantaneous axis of rotation of the solid Earth relative to its axis of figure, as specified by the quantity

$$m(t) \equiv m_1(t) + i m_2(t) \quad (\text{A6b})$$

where $i \equiv \nu - 1$. See equation (A3). Indeed, the strongest torques acting on the solid Earth are generated by atmospheric motions, which produce easily detectable changes in A of up to about 1 ms in magnitude (corresponding to change in $|m_3|$ of about 10^{-8}) and displacements of the pole of rotation of several metres (corresponding to changes in $|m|$ of about 10^{-6}).

The torque $-L_i$ produced by atmospheric motions on the underlying planet is due to (a) tangential stresses in the turbulent boundary layers over the continents and oceans, and (b) normal stresses acting on orography and the Earth's equatorial bulge. Owing to the rigidity (albeit slightly imperfect) of the solid Earth, all three components of the 'continental' part of $-L_i$ are transmitted to the solid Earth directly and fully. The oceanic part of $-L_i$ gives rise to a dynamical response in the oceans which requires further investigation, but the case when the whole of the applied torque is assumed to be passed on by the oceans to the solid Earth virtually instantaneously can be taken as realistic for most practical purposes, particularly when dealing with the axial component of $-L_i$ and the changes in A that it produces [Ponte, 1990]. Thus, the oceans act as an intermediary in the angular momentum exchange process, by transmitting the applied stresses in the atmospheric boundary layer over the oceans to the continental margins and ocean bottom. It is a convenient circumstance that, owing to the slowness and scales of ocean currents in comparison with atmospheric winds, in the budget of angular momentum between the solid Earth and its overlying fluid layers, the hydrosphere (in spite of its much greater

moment of inertia than that of the atmosphere, by a factor of about 300) produces effects which can be neglected to a first approximation.

In the theory of the interactions between the atmosphere and underlying planet that give rise to fluctuations in M_i , the analysis is facilitated by using in place of M_i the dimensionless AAM functions χ_i , $i = 1, 2, 3$, (see Barnes *et al.*, 1983). They can be defined as follows:

$$\chi_i \equiv \chi_i^P + \chi_i^W = \int_{-\pi/2}^{\pi/2} \xi_i(\phi, t) d\phi = \int_{-\pi/2}^{\pi/2} [\xi_i^P(\phi, t) + \xi_i^W(\phi, t)] d\phi, \quad (\text{A7})$$

where $(\xi_1^P, \xi_2^P) \equiv \frac{-1.098\bar{R}^4}{g(C-A)} \int_0^{2\pi} p_s \cos^2 \phi \sin \phi (\cos \lambda, \sin \lambda) d\lambda$ (A8a)

$$(\xi_1^W, \xi_2^W) \equiv \frac{-1.5913\bar{R}^3}{g(C-A)\Omega} \iint_{00}^{P_2\pi} \cos \phi \{ u \sin \phi (\cos \lambda, \sin \lambda) - v (\sin \lambda, -\cos \lambda) \} d\lambda dp, \quad (\text{A8b})$$

and

$$(\xi_3^P, \xi_3^W) = \left(\frac{0.753\bar{R}^4}{gC_m} \int_0^{2\pi} p_s \cos^3 \phi d\lambda, \frac{0.998\bar{R}^3}{gC_m\Omega} \iint_{00}^{P_2\pi} u \cos^2 \phi d\lambda dp \right). \quad (\text{A9})$$

In these expressions, (ϕ, λ) denote latitude and longitude respectively, $p_s(\phi, \lambda, t)$ is the surface pressure and $u(\phi, \lambda, p, t)$ and $v(\phi, \lambda, p, t)$ are the eastward and northward components respectively of the wind velocity at pressure level p . We take $\bar{R} = 6.3674 \times 10^6$ m for the mean radius of the solid Earth, $\Omega = 7.292115 \times 10^{-5}$ rad s^{-1} for its mean rotation rate, $g = 9.810$ m S^{-2} for the mean acceleration due to gravity, $C = 8.0376 \times 10^{37}$

kg m² for the polar moment of inertia of the whole Earth, $(C-A) = 2.610 \times 10^{35}$ kg m² where A is the corresponding equatorial moment of inertia, and $C_m = 7.1236 \times 10^{37}$ kg m² is the polar moment of inertia of the Earth's mantle and crust. The coefficients 1.098, 1.5913, 0.753, and 0.998 incorporate the so-called 'Love number' corrections, which allow for concomitant meteorologically-induced tiny but dynamically significant changes in the inertia tensor of the slightly deformable solid Earth, using the most up-to-date geophysical data (see Eubanks, 1993). The dimensionless pseudo-vector χ_i is related to the AAM vector M_i , with the equatorial components (χ_1, χ_2) and (M_1, M_2) scaled differently from the axial components χ_3 and M_3 . Routine determinations of χ_i have been made for several years at several meteorological centers (using older values of the "Love number" corrections, namely 1.00, 1.43, 0.70 and 1.00 respectively in place of 1.098, 1.5913, 0.753 and 0.998, C_m in place of C and A_m in place of A in equations (A8)).

Any change in M_3 is accompanied by an equal and opposite change in the axial component of the angular momentum of the solid Earth (since the fluctuations in the azimuthal motion of the underlying liquid core of moment of inertia $\sim 0.1 C$ are effectively decoupled from those of the solid Earth on the short time scales with which we are concerned here). In terms of the dimensionless quantities m_3 and χ_3 this can be expressed as

$$\dot{m}_3 + \dot{\chi}_3 = 0 \tag{A10}$$

with solution
$$m_3(t) + \chi_3(t) = m_3(t_0) + \chi_3(t_0), \tag{A11}$$

where $m_3(t_0)$ and $\chi_3(t_0)$ are constants of integration equal respectively to m_3 and χ_3 at some initial instant $t = t_0$. The dominant contribution to fluctuations in χ_3 comes from the 'wind' term χ_3^w , which depends on the distribution in the meridional plane of the average

with respect to longitude λ of the eastward (westerly) wind speed. If one considers only the wind contribution, equation (A7) for the axial component simplifies to

$$\chi_3^w = \frac{0.998(2\pi)\bar{R}^3}{gC_m\Omega} \int_0^P \int_{-\pi/2}^{\pi/2} [u] \cos^2 \phi \, d\phi \, dp. \quad (\text{A12})$$

in which case M_3 , the axial atmospheric angular momentum, reduces to

$$M_3^w = 2\pi g^{-1} \bar{R}^3 \int_0^P \int_{-\pi/2}^{\pi/2} [u] \cos^2 \phi \, d\phi \, dp. \quad (\text{A13})$$

REFERENCES

- Anderson, J. D., and R.D. Rosen, The latitude-height structure of 40-50 day variations in atmospheric angular momentum, *J. Atmos. Sci.*, 40, 1584-1591, 1983.
- Barnes, R. T. H., R. Hide, A. A. White, and C. A. Wilson. Atmospheric angular momentum fluctuations, length of day changes and polar motion, *Proc. R. Soc. Lon.*, A387, 31-73, 1983.
- Bell, M. J., R. Hide, and G. Sakellarides, Atmospheric angular momentum forecasts as novel tests of global numerical prediction models, *Phil. Trans R. Soc. Lon.*, A334, 55. 92, 1991.
- Boer, G. J., Earth-atmosphere exchange of angular momentum simulated in a general circulation model and implications for the length-of-the-day, *J. Geophys. Res.*, 95. 5511-5531, 1990.
- Chao, B. F., Interannual length of day variations with relation to the Southern Oscillation/El Niño, *Geophys. Res. Letts.*, 11, 541-544, 1984.
- Chao, B. F., Correlation of interannual lengths-of-day variation with El Niño/Southern oscillation, 1972-1986, *J. Geophys. Res.*, 93, B7, 7709-7715, 1988.
- Chao, B. F., Length-of-day variations caused by El Niño/Southern Oscillation and the Quasi-Biennial oscillation, *Science*, 24.3, 923-925, 1989.

Dickey, J. O., Atmospheric excitation of the earth's rotation: Progress and prospects via space geodesy, in *Contributions of Space Geodesy to Geodynamics, Earth Dynamics*, edited by D. E. Smith and D. L. Turcotte, *Am. Geophys. Un.*, Washington, D.C., S5-70, 1993.

Dickey, J. O., M. Ghil, and S. I. Marcus, Extratropical aspects of the 40-50 day oscillation in length of day and atmospheric angular momentum, *J. of Geophys. Res.* 96,22,643-22,658, 1991.

Dickey, J. O., S. I. Marcus, and R. Hide, Global propagation of interannual fluctuations in atmospheric angular momentum, *Nature*, 357, 484-488, 1992.

Dickey, J. O., S. I. Marcus, T. M. Eubanks, and R. Hide, Climate studies via space geodesy: Relationships between ENSO and interannual length-of-day variations, in *Interactions Between Global Climate Subsystems: The Legacy of Hann*, *Geophys. Monogr. Ser.*, vol. 75, edited by G. A. McBean and M. Hantel, pp. 141-155, AGU, Washington, D.C., 1993a.

Dickey, J. O., S. I. Marcus, C. M. Johns, R. Hide, S. R. Thompson, The oceanic contribution to the earth's seasonal angular momentum budget, *Geophys. Res. Lett.*, 20,2953-2956, 1993.

Dickey, J. O., S. I. Marcus, R. Hide, T. M. Eubanks, and D. H. Boggs, Angular momentum exchange among the solid earth, atmosphere, and oceans: A case study of the 1982-1983 El Niño event, *J. Geophys. Res.*, 99, 23,921-23,937, 1994.

Eubanks, T. M., Variations in [the orientation of the Earth, in *Contribution of Space Geodesy and Geodynamics: Earth Dynamics, Geodyn. Ser.*, vol. 24, edited by D. E. Smith and D. L. Turcotte, pp. 1-54, American Geophysical Union Monograph, Washington D. C., 1993.

Eubanks, T. M., J. A. Steppe, and J. O. Dickey, The El Niño, the Southern Oscillation and the Earth's Rotation, in *Earth Rotation: Solved and Unsolved Problems, NATO Advanced Institute Series C: Mathematical and Physical Sciences, 187, cd. A. Cazenave*, 163-186, D. Reidel, Hingham, Mass., 1986.

Fiorino, M., AMIP Overview—An Analysis of the Base State, in *Proceedings of the First International AMIP Scientific Conference*, 15-19 May, 1995, Monterey, CA, WCRP-92, WMO/TD-No. 732,531, 1995.

Gates, W.L., AMIP: "The Atmospheric Model Intercomparison Project, *Bull. Amer. Meteor. Sm.*, 73, 1962-1970, 1992.

Hide, R., N. T. Birch, L. V. Morrison, D. J. Shea, and A. A. White, Atmospheric angular momentum fluctuations and changes in the length of the day, *Nature*, 286, 14-17, 1980.

Hide, R. and J. O. Dickey, Earth's variable rotation, *Science*, 253, 629-637, 1991

Jordi, C., L. V. Morrison, R. D. Rosen, D. A. Salstein, and G. Rossi, Fluctuations in the earth's rotation since 1830 from high resolution astronomical data, *Geophys. J. Int.*, 117, 811-818, 1994.

- Kim, Y.-J., Representation of subgrid-scale orographic effects in a general circulation model: Impact on the dynamics of simulated January climate, *J. Clim.*, submitted, 1996.
- Kim, Y.-J., and A. Arakawa, Improvement of orographic gravity-wave parameterization using a mesoscale gravity-wave model, *J. Atmos. Sci.*, *52*, 1875-1902, 1995.
- Lanzante, J.R., Resistant, robust and nonparametric techniques for the analysis of climate data: Theory and examples, including applications to historical radiosonde station data, submitted manuscript, 1996.
- Marcus, S. L., M. Ghil, and J. O. Dickey, The Extratropical 40-day oscillation in the UCLA general circulation model, Part 1: Atmospheric angular momentum, *J. Atmos. Sci.*, *51*, 1431-1466, 1994.
- Marcus, S. L., M. Ghil, and J. O. Dickey, The Extratropical 40-day oscillation in the UCLA general circulation model, Part 11: Spatial structure, *J. Atmos. Sci.*, accepted, 1995.
- Marcus, S. L., and J. O. Dickey, Coupled poleward propagation of sea surface temperature and atmospheric angular momentum anomalies: Results from AM II', *Sixth Conference on Climate Variations*, American Meteorological Society, 70-74, 1994a.
- Phillips, T. J., *A Summary Documentation of the AMIP Model.Y*, PCMDI Report No. 18, Program for Climate Model Diagnosis and Intercomparison, Lawrence Livermore National Laboratory, Livermore, CA, 343 pp, 1994.

Ponte, R. M., Barotropic motions and the exchange of angular momentum between the oceans and solid earth, *J. Geophys. Res.*, 95, 11,369-11, 374, 1990.

Ponte, R. M., R. D. Rosen, and G. J. Boer, Angular momentum and torques in a simulation of the atmosphere's response to the 1982-83 El Niño, *J. Climate*, 7, 538-550, 1994.

Rosen, R.D., The axial momentum balance of earth and its fluid envelope, *Geophys.*, 14, 1-29, 1993.

Rosen, R. D. and D.A. Salstein, Contribution of stratospheric winds to annual and semi-annual fluctuations in atmospheric angular momentum and the length of day, *J. Geophys. Res.*, 90, 8033-8041, 1985.

Rosen, R. D., and D.A. Salstein, Variations in atmospheric angular momentum on global and regional scales and the length of day, *J. Geophys. Res.*, 88, 5451-5470, 1983.

Rosen, R. D., D. A. Salstein, J. M. Eubanks, J. O. Dickey, and J. A. Steppe, An El Niño signal in atmospheric angular momentum and earth rotation, *Science*, 225, 411-414, 1984.

Rosen, R. D., D.A. Salstein, and T. Nehr Korn, Predictions of zonal wind and angular momentum by the NMC Medium-Range Forecast Model during 1985-89, *Mon. Wea. Rev.*, 119, 208-217, 1991a.

- Rosen, R. D., D. A. Salstein, and T. M. Wood, Zonal contributions to global momentum variations on intraseasonal through interannual time scales, *J. Geophys. Res.*, 96, 5145-5151, 1991b.
- Rosen, R. D., D. A. Salstein, and T. M. Wood, Discrepancies in the earth-atmosphere angular momentum budget, *J. Geophys. Res.*, 95, 265-279, 1990.
- Rosen, R. D., D. A. Salstein, A. J. Miller, and K. Arpe, Accuracy of atmospheric angular momentum estimates from operational analyses, *Mon. Wea. Rev.*, 115, 1627-1639, 1987.
- Salstein, D. A., and R. D. Rosen, Topographic forcing of the atmosphere and a rapid change in the length-of-day, *Science*, 264, 407-409, 1994.
- Salstein, D. A., and R. D. Rosen, Earth rotation as a proxy for interannual variability in atmospheric circulation, 1980-present, *J. Clim. Appl. Meteorol.*, 25, 1870-1877, 1986.
- Salstein, D. A., D. M. Kann, A. J. Miller, and R. D. Rosen, The Sub-Bureau for Atmospheric Angular Momentum of the International Earth Rotation Service (IERS): A meteorological data center with geodetic applications, *Bull. Am. Met. Soc.* 74, 67-80, 1993.
- White, G. H., in "Proceedings of the American Geophysical Union Chapman Conference on Geodesy VI: Monitoring Global Change," *Nat. Oceanic Atmos. Adm. Tech. Rep. NOS 137 NC; S 49*, 262, 1991.

March 18, 1996

White, G. H., in "Research Activities in Atmospheric and Oceanic Modeling," *CAS/JSC Work Group Numer. Exp. Rep. no. 18* (World Meteorological Organization, Geneva, 2.3-2.4, 1993).

LEGENDS FOR FIGURES

Figure 1. Time series of irregular fluctuations in the length of the day (LOD) from 1963 to 1992 (curve a) and its decadal, interannual, seasonal, and intraseasonal components (curves b, c, d and e, respectively). The decadal (curve b) component largely reflects angular momentum exchange between the solid Earth and the underlying liquid metallic outer core produced by torques acting at the core-mantle boundary. The other components (curves c, d and e) largely reflect angular momentum exchange between the atmosphere and [he solid Earth, produced by torques (proportional to the time-derivative of the LOD time series) acting directly on the solid Earth over continental regions of the Earth's surface and indirectly over oceanic regions (adapted from Hide and Dickey, 1991).

Figure 2. The axial component of atmospheric angular momentum (M^W), determined from the monthly standard output for 23 AMIP models which extends up to the 50 mb level (solid lines). The dashed and dotted lines (repeated in each panel) show respectively M^W determined from the operational NMC analysis for the AMIP decade, and global angular momentum fluctuations inferred from geodetic data (a quadratic offset has been removed from the geodetic LOD determinations to account for core-mantle effects). 1 cmsu (equivalent millisecond unit) of axial angular moment corresponds to $0.67 \times 10^{26} \text{ kg m}^2 \text{ s}^{-1}$.

Figure 3. Mean value of the relative angular momentum of the atmosphere between 1000 mb and 50 mb during the decade, 1979-88 for each of 23 models. At the right are plotted the median and the upper and lower quartiles of the distribution of model values, with the length of the vertical line connecting the last two depicting the interquartile range. The

dashed line indicates the value observed for the same. decade based cm NMC operational analyses.

Figure 4a. Meridional cross section of the average value of the zonal-mean zonal wind observed during the decade 1979-88 based on NMC operational analyses. Standard pressure levels marked along the ordinate correspond to the vertical distribution of the archived analyses. Shaded values are negative (easterlies). The global-mean value of the $[u]$ field shown here is 6.8 ms^{-1} .

Figure 4b. Meridional cross sections of the average value of the zonal-mean zonal wind during the decade 1979-88 for four selected models minus the observed value from Figure 4a. In the left column are the models with the two largest values of M^w in Figure 3; the right column contains the models with the two smallest values of M^w in Figure 3. Negative values are shaded.

Figure 5. Meridional cross section of the average value of the zonal-mean zonal wind during the decade 1979-88 for the GLA model minus the observed value from Figure 4a. Negative values are shaded.

Figure 6. The three leading empirical orthogonal functions (EOF's) of the covariance matrix formed from the 23 model time series of the difference between the decadal-mean model value of the relative angular momentum in each of 46 equal-area belts (m_b^w) and the observed value. The eigenvector on the left is plotted in units of $10^{24} \text{ kg m}^2 \text{ s}^{-1}$. The weight contributed by each model to each of the EOF's is given on the right in nondimensional, normalized units; the models are shown in the same sequence as in Figure 3. The percent of the variance in all the model's belt momentum biases explained by each EOF is also shown.

Figure 7. The median among the 23 model values of the relative angular momentum of the atmosphere between 1000 and 50 mb for each composite calendar month of 1979-88 (solid line), along with the upper and lower quartiles of the distribution of model values for each composite month. The dashed line indicates the observed composite monthly values, based on NMC operational analyses. The decadal mean of the series for each model and for the observations has been removed prior to generating these results.

Figure 8. The first two empirical orthogonal functions of the covariance matrix formed from the 23 models' time series of their composite monthly values of M^w minus the observed value. The eigenvector on the left is plotted in units of $10^{24} \text{kgm}^2\text{s}^{-1}$. The weight contributed by each model to each of the modes is given on the right in nondimensional, normalized units; the models are shown in the same sequence as in Figure 3. The percent of the variance in all the models' seasonal errors explained by each mode is also shown.

Figure 9. At bottom, the standard deviation of the twelve composite calendar-month means during 1979-88 of the relative angular momentum of the atmosphere between 1000 and 50 mb (M^w) for each of 23 models. To the right on the same scale are plotted the median and the upper and lower quartiles of the distribution of model values. The dashed line indicates the value observed for the same decade based on NMC operational analyses. At top, the correlation coefficient (scale on right) between each model's series of composite monthly M^w values and the observed series.

Figure 10(a). The variance observed in the composite calendar-month values of the relative angular momentum in each of 46 equal-area belts (m_b^w), based on NMC operational analyses for 1979-1988. (b). The median among the 23 model values of the

variance in the difference between a model's composite monthly mean series of m_b^w and the observed m_b^w series, along with the upper and lower quartiles of the distribution of the 23 model values of this error variance for each belt. (c). The median among the 23 model values of the covariance between the seasonal errors in a model's series of m_b^w (i.e., the difference between its composite monthly mean series of m_b^w and the observed m_b^w series) and the seasonal errors in its series of M^w (i. e., the difference between the model's composite monthly mean series of M^w and the observed M^w series), divided by the variance in the difference between the model's composite monthly mean series of M^w and the observed M^w series. Also plotted are the upper and lower quartiles of the distribution of the 23 model values of this fractional error covariance for each belt.

Figure 11. As in Figure 7. but for the interannual component of the relative angular momentum of the atmosphere between 1000 and 50 mb (M^w) formed by averaging monthly values of M^w in each of 40 seasons during 1979-1988 and subtracting from this series the decadal mean seasonal cycle.

Figure 12. As in Figure 9, but for the interannual component of the relative angular momentum of the atmosphere between 1000 and 50 mb (M^w) formed by averaging monthly values of M^w in each of 40 seasons during 1979-1988 and subtracting from this series the decadal mean seasonal cycle.

Figure 13. (a) As in Figure 10 a and b, but for the interannual component of the relative angular momentum in each of 46 (qua)-area belts (m_b^w) formed by averaging monthly values of m_b^w in each of 40 seasons during 1979-1988 and subtracting from this series the decadal mean seasonal cycle. (b) As in Figure 10c, but for the interannual component.

Table 1
List of AMIP Models inter'compared in this study together with an
indication of their performance*

		Decadal Mean	Sea- sonal σ_s	Inter- annual σ_I
MRC	Bureau of Meteorology Research Centre (Australia)	√	√	√
CCC	Canadian Centre for Climate Research	√	√	√
CNRM	Centre National de Recherches Météorologiques (France)	—	√	√
CSIRO	Commonwealth Scientific and Industrial Research Organization (Australia)	√	√	·
DERF	Dynamical Extended-Range Forecasting (at GFDL)	√	√	+
DNM	Department of Numerical Mathematics (of the Russian Academy of Sciences)	—	+	—
ECMWF	European Centre for Medium-Range Weather Forecasts	√		√
GIIL	Geophysical Fluid Dynamics laboratory	√	+	√
GLA	Goddard Laboratory for Atmospheres, NASA	√	√	√
GSFC	Goddard Space Flight Center, NASA	√	√	·
IMA	Japan Meteorological Agency	√	+	√
MGO	Main Geophysical observatory, Russia	√	+	√
MIJ	Max-Planck-Institut für Meteorologie, Germany	√	-	+
MRI	Meteorological Research Institute, Japan	√	√	—
NCAR	National Center for Atmospheric Research	+	+	·
NMC	National Meteorological Center (now NCEP)			√
NRL	Naval Research Laboratory, Monterey	√	-	+
RPN	Recherche en Prévision Numérique, Canada	√		—
SNG	State University of New York at Albany/NCAR	√	+	·
SUNYA	State University of New York at Albany	√	√	·
UCI/A	University of California at Los Angeles	·		
UGAMP	The UK Universities' Global Atmospheric Modelling Programme	√	√	√
UKMO	United Kingdom Meteorological Office	√	+	+

* See the three columns on the right, where \checkmark indicates that the model gives a value within 15% of that observed, --- a value more than 15% lower than observed and + more than 15% higher.

Figure 1

COMPONENT N-1 OF (t)

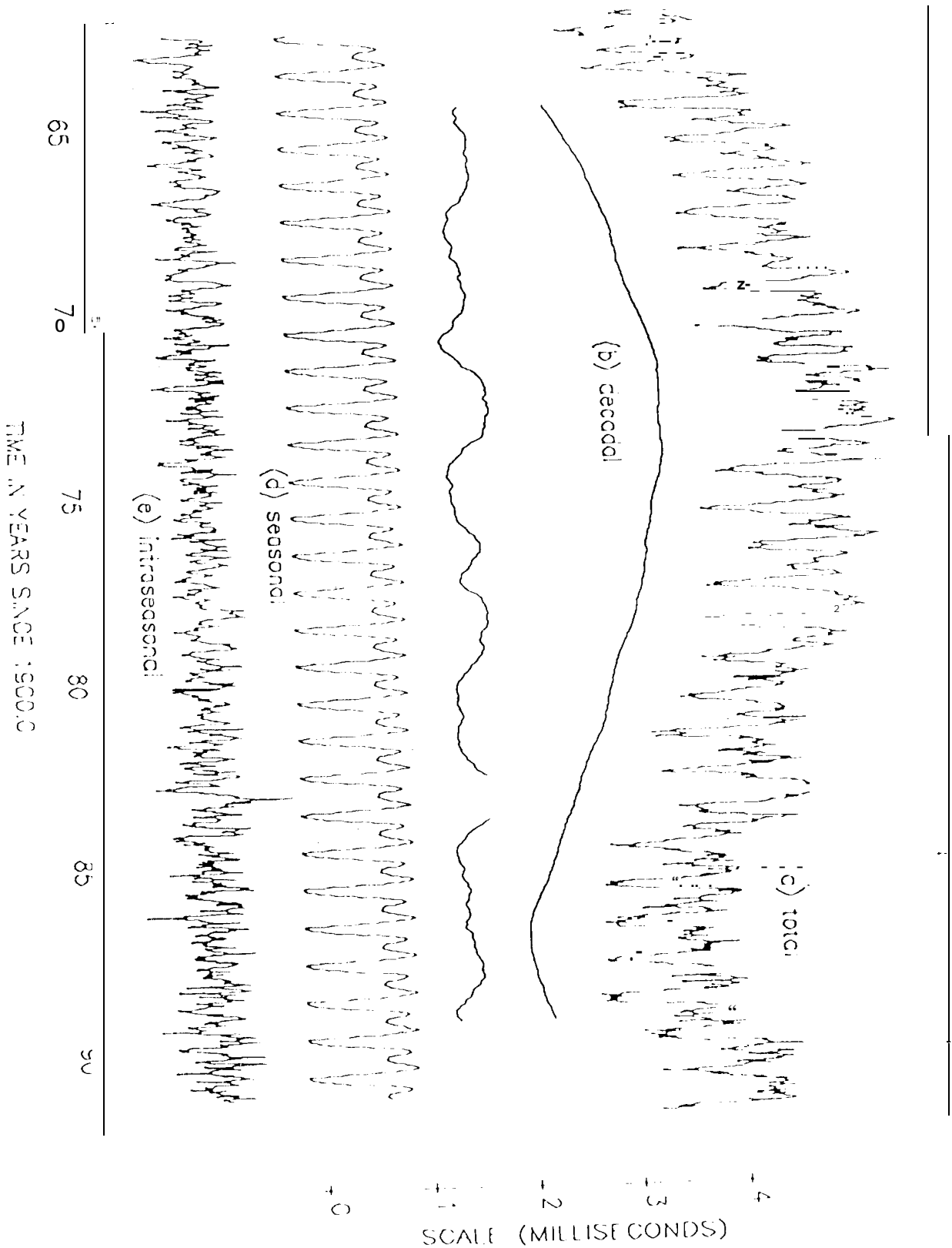


Figure 2

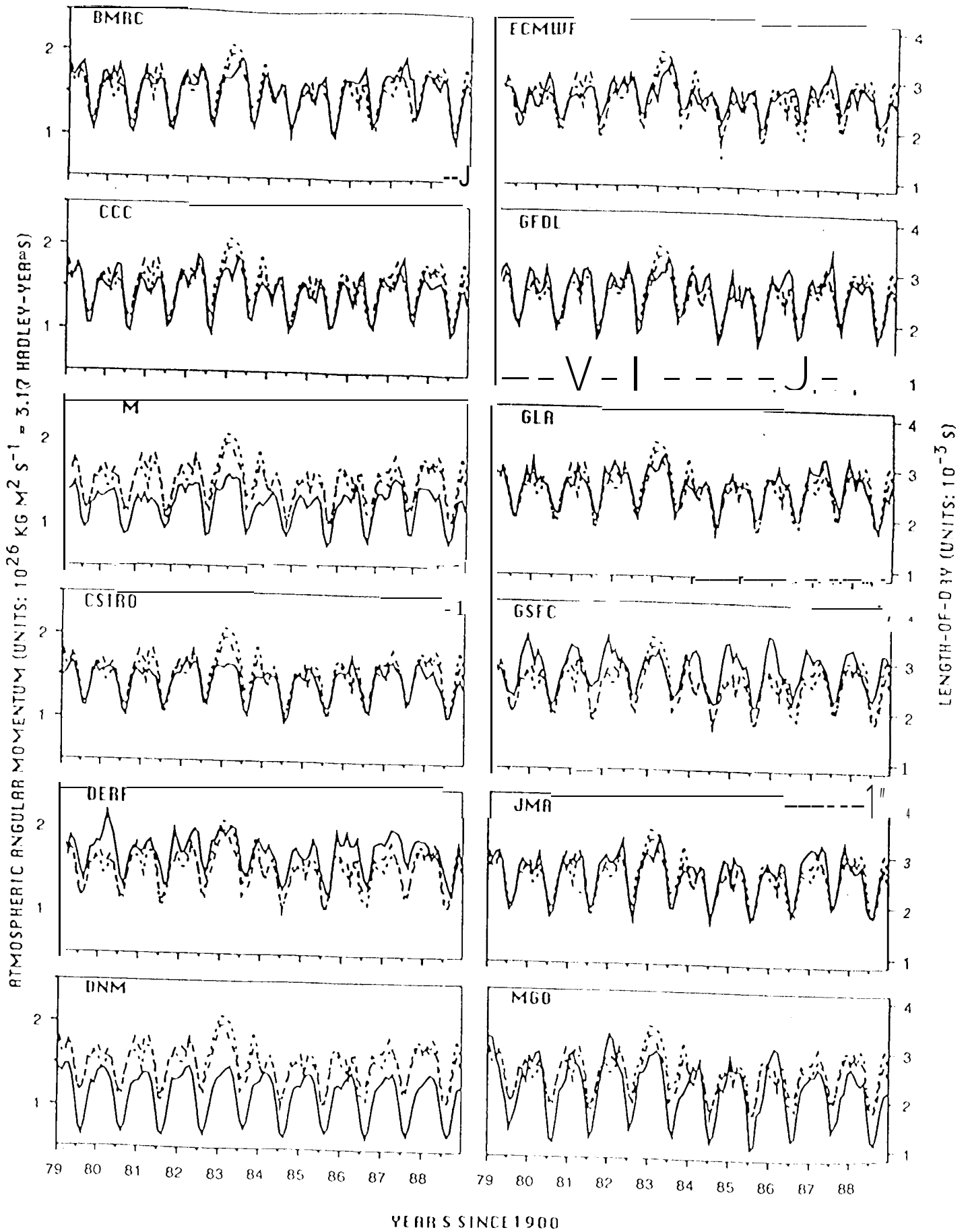


Figure 2 cont.

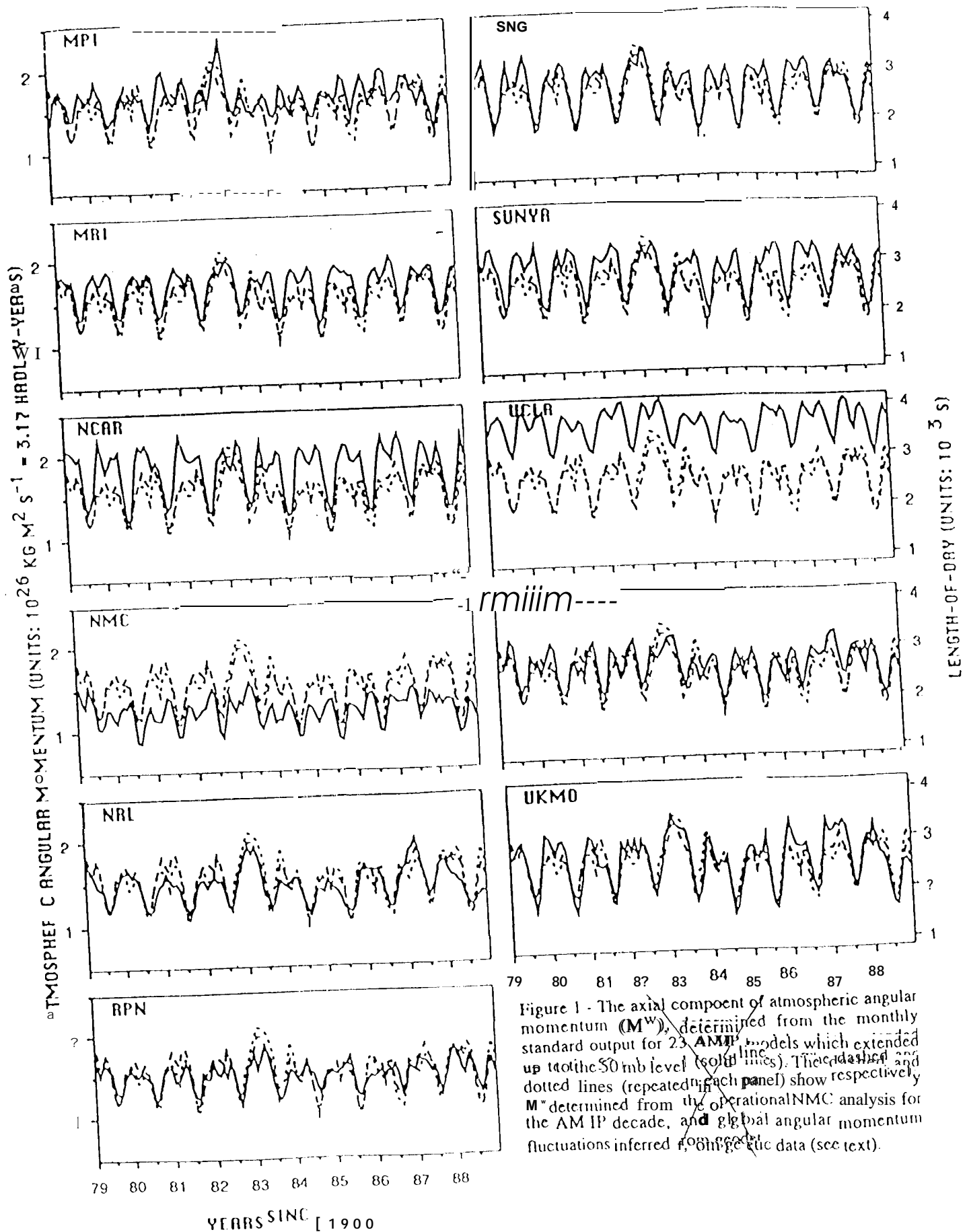


Figure 1 - The axial component of atmospheric angular momentum (M^w), determined from the monthly standard output for 23 AMIP models which extended up to the 50 mb level (solid lines). The dashed and dotted lines (repeated in each panel) show respectively M^w determined from the operational NMC analysis for the AMIP decade, and global angular momentum fluctuations inferred from geologic data (see text).

Figure 3

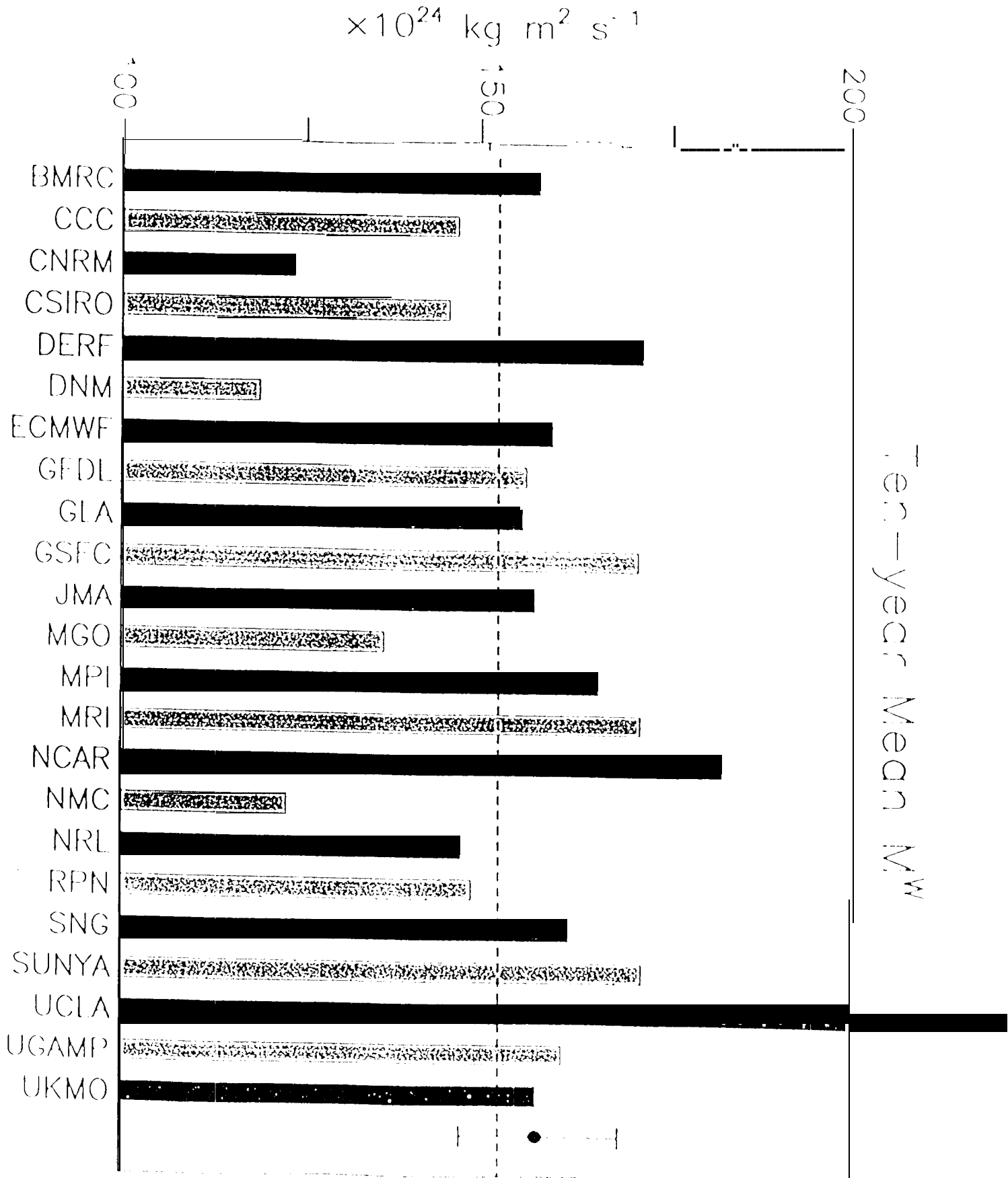


Figure 4a

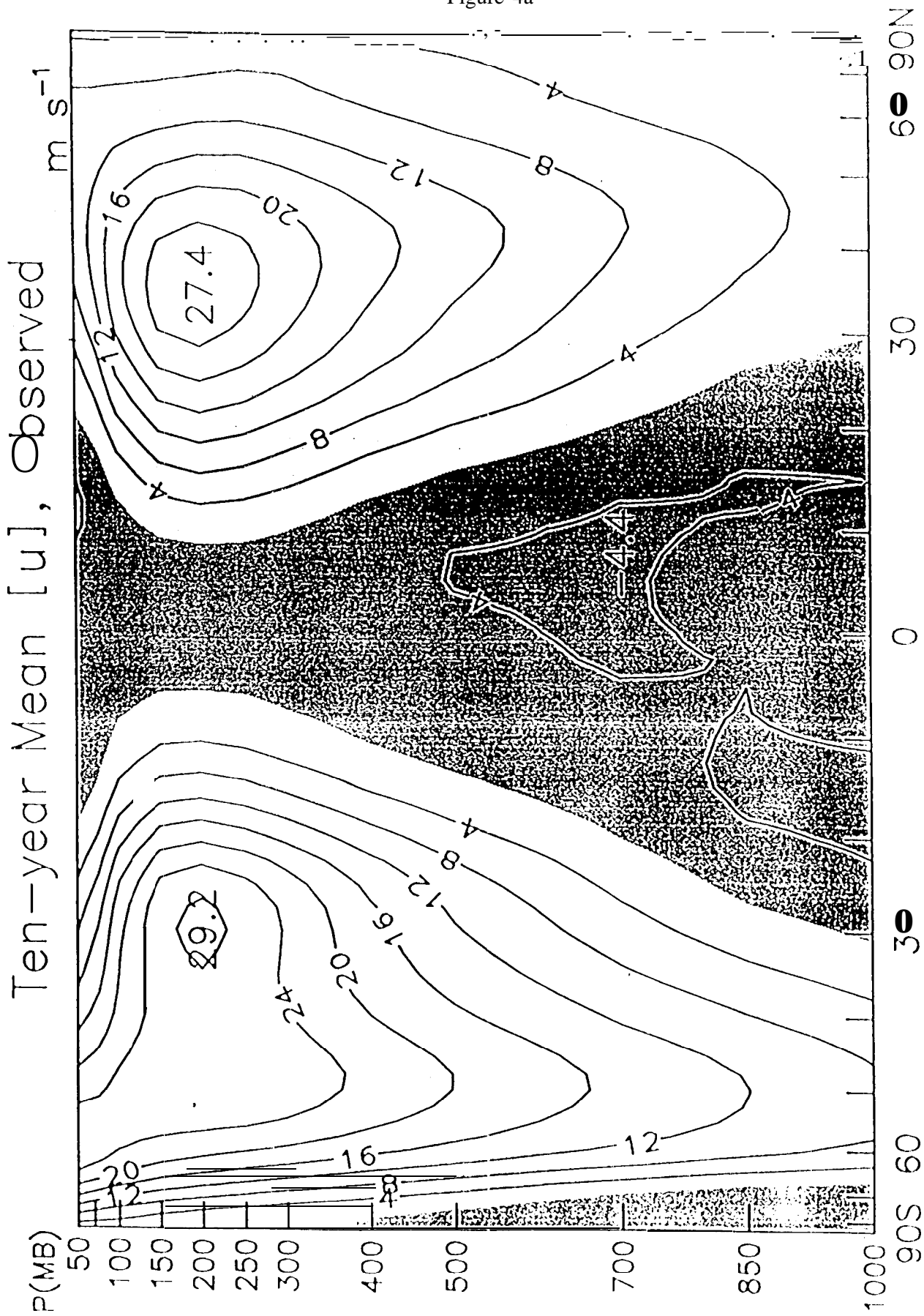
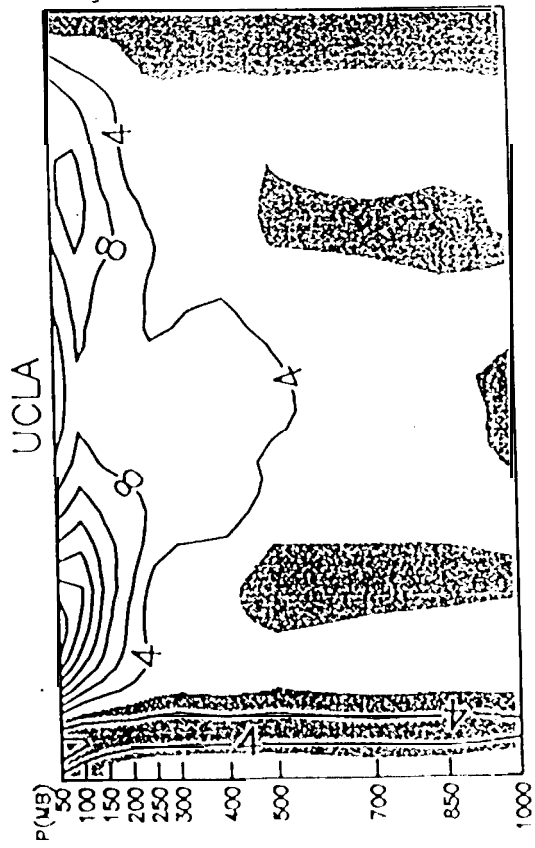
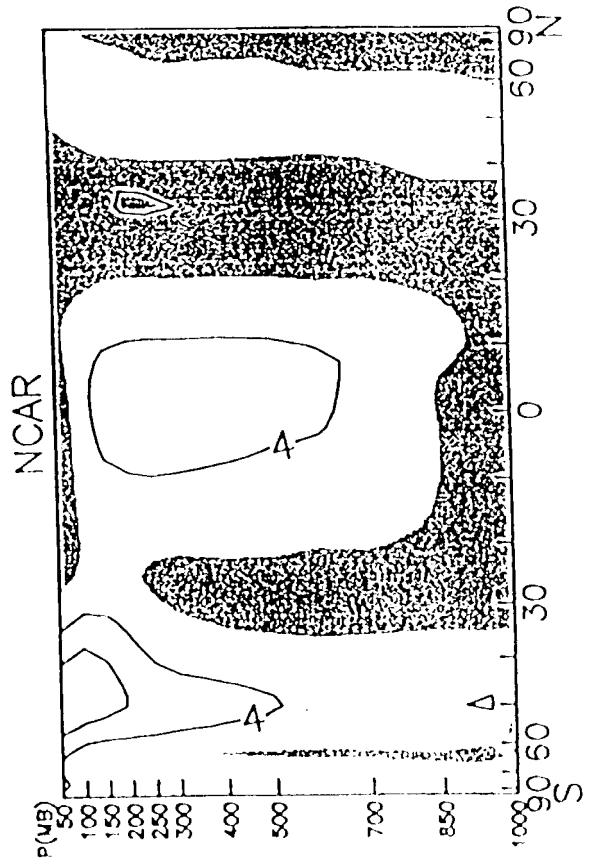
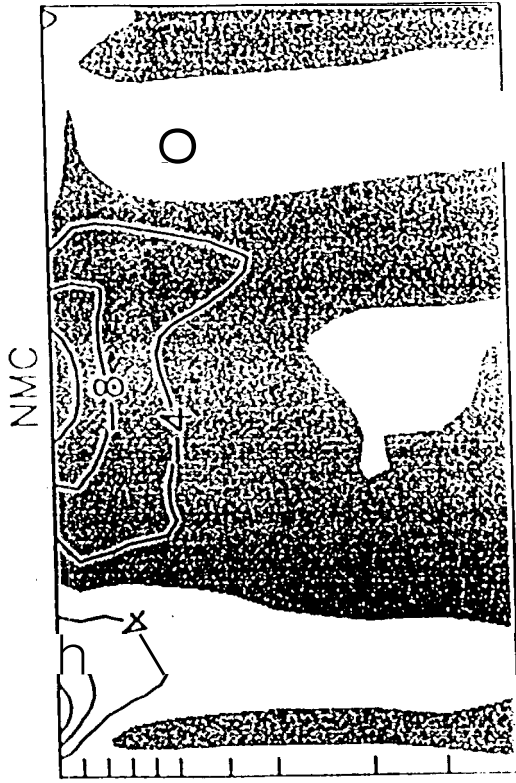


Figure 4b

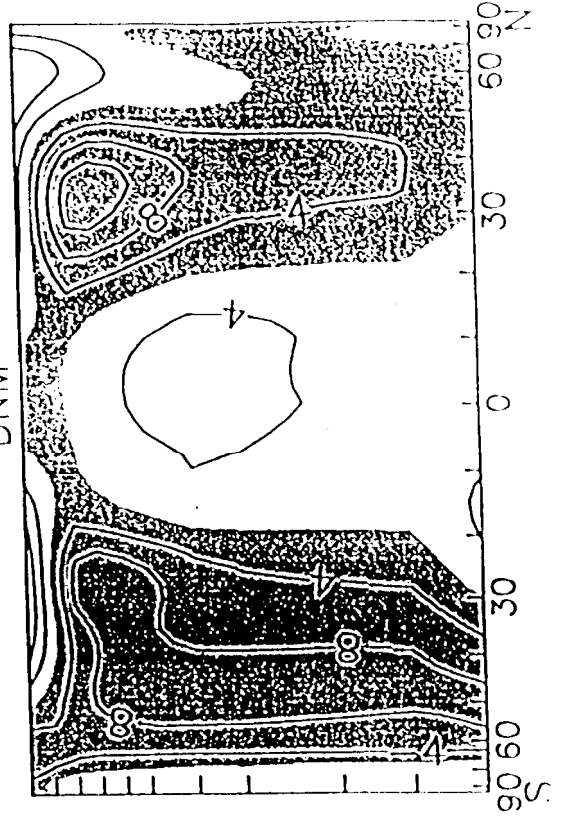
Ten-Year Mean [u] Bias ($m s^{-1}$)
 M^W Very High



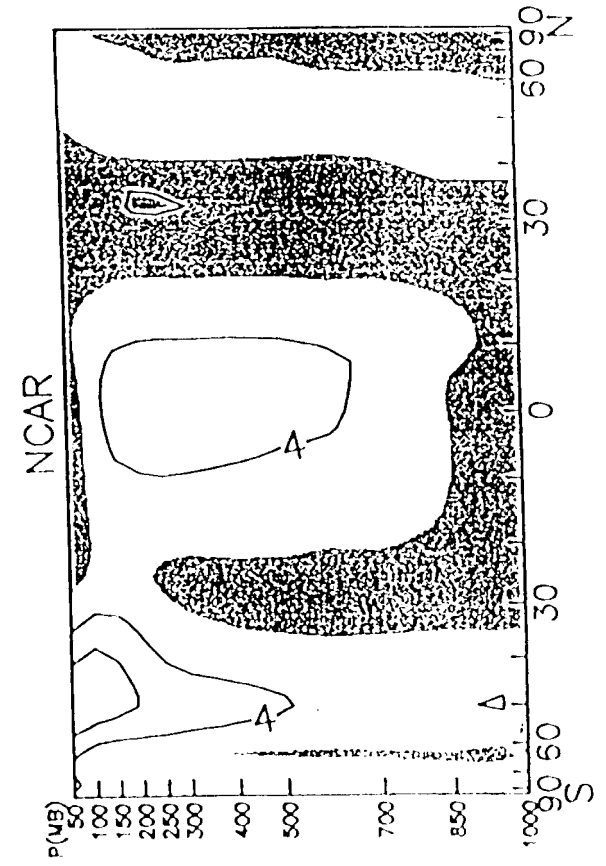
M^W Very Low



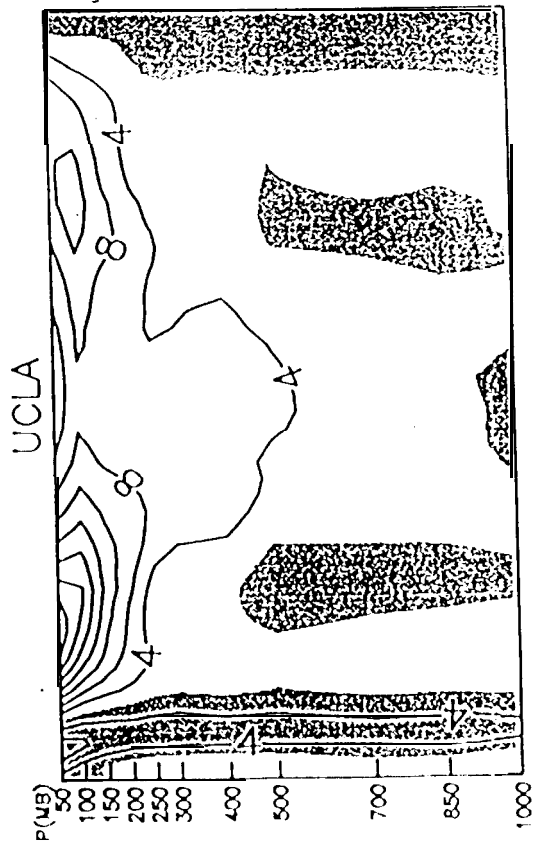
DNM



NCAR



UCLA



NMC

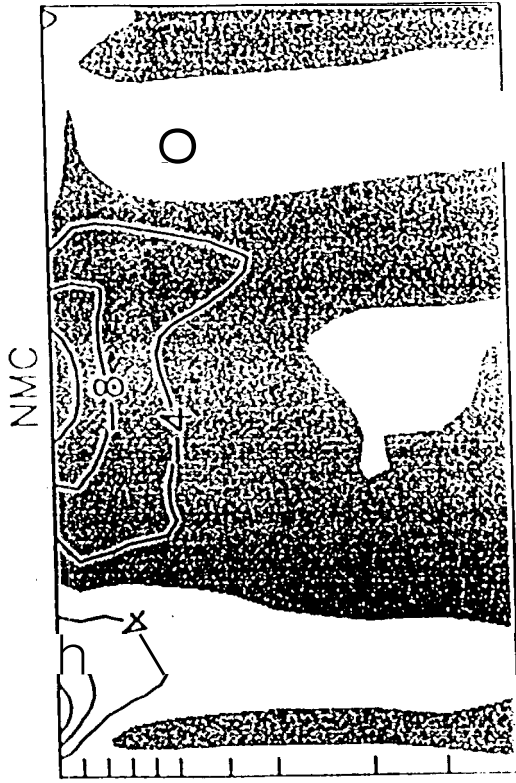
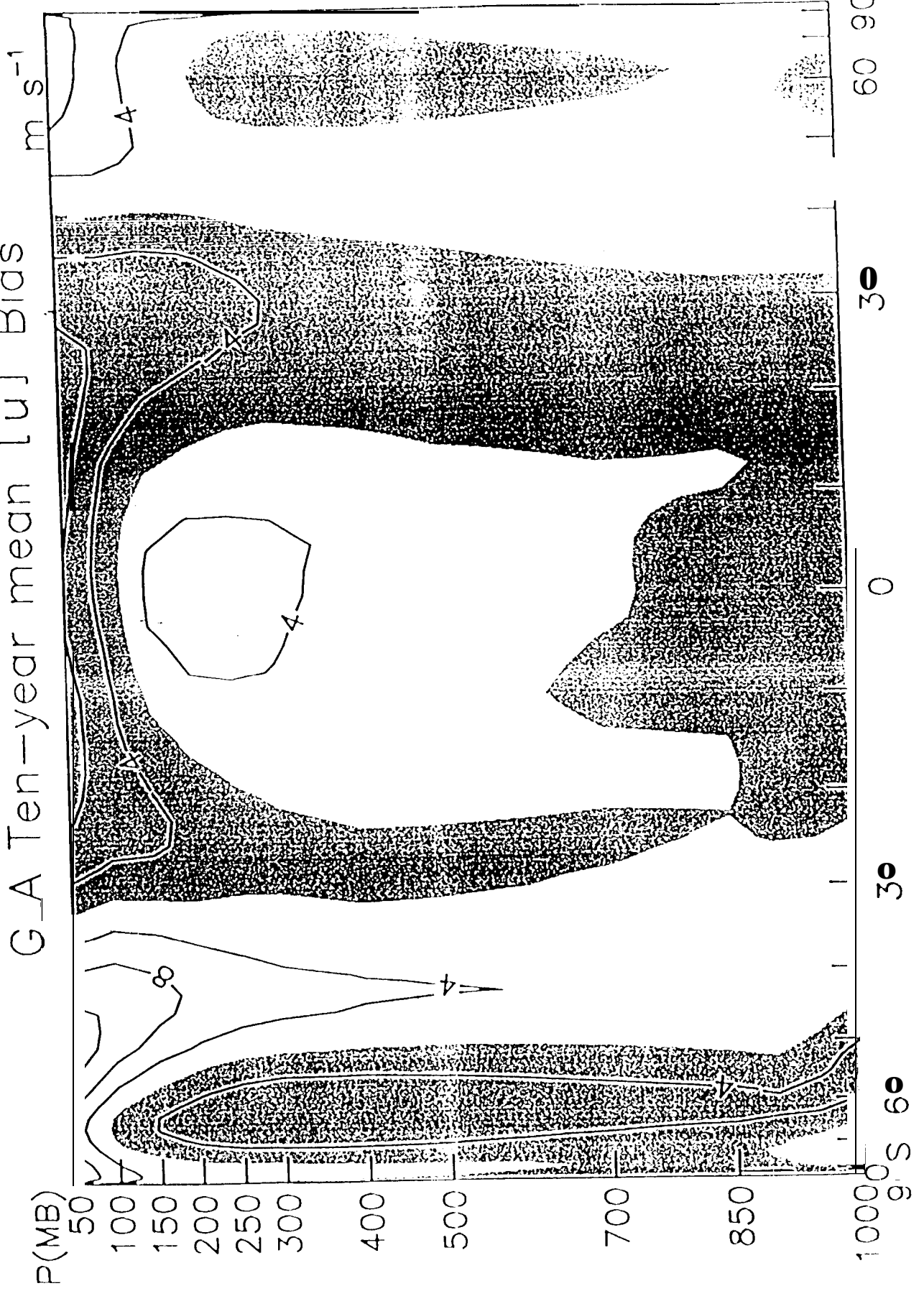


Figure 5

G_A Ten-year mean [u] Bias



Spatial Modes of Be Momentum Biases

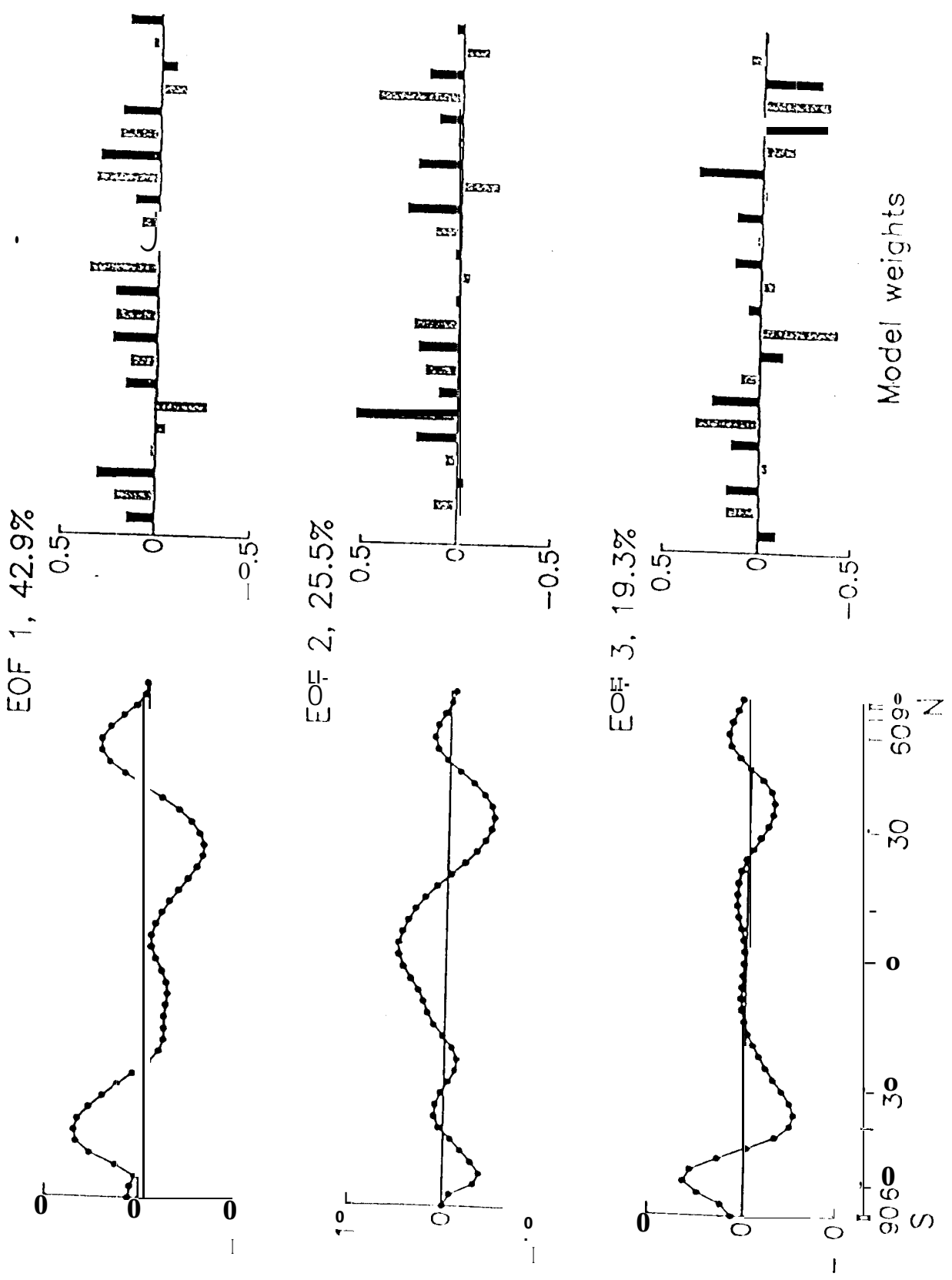


Figure 6

Figure 7

M^W , Seasonal Component

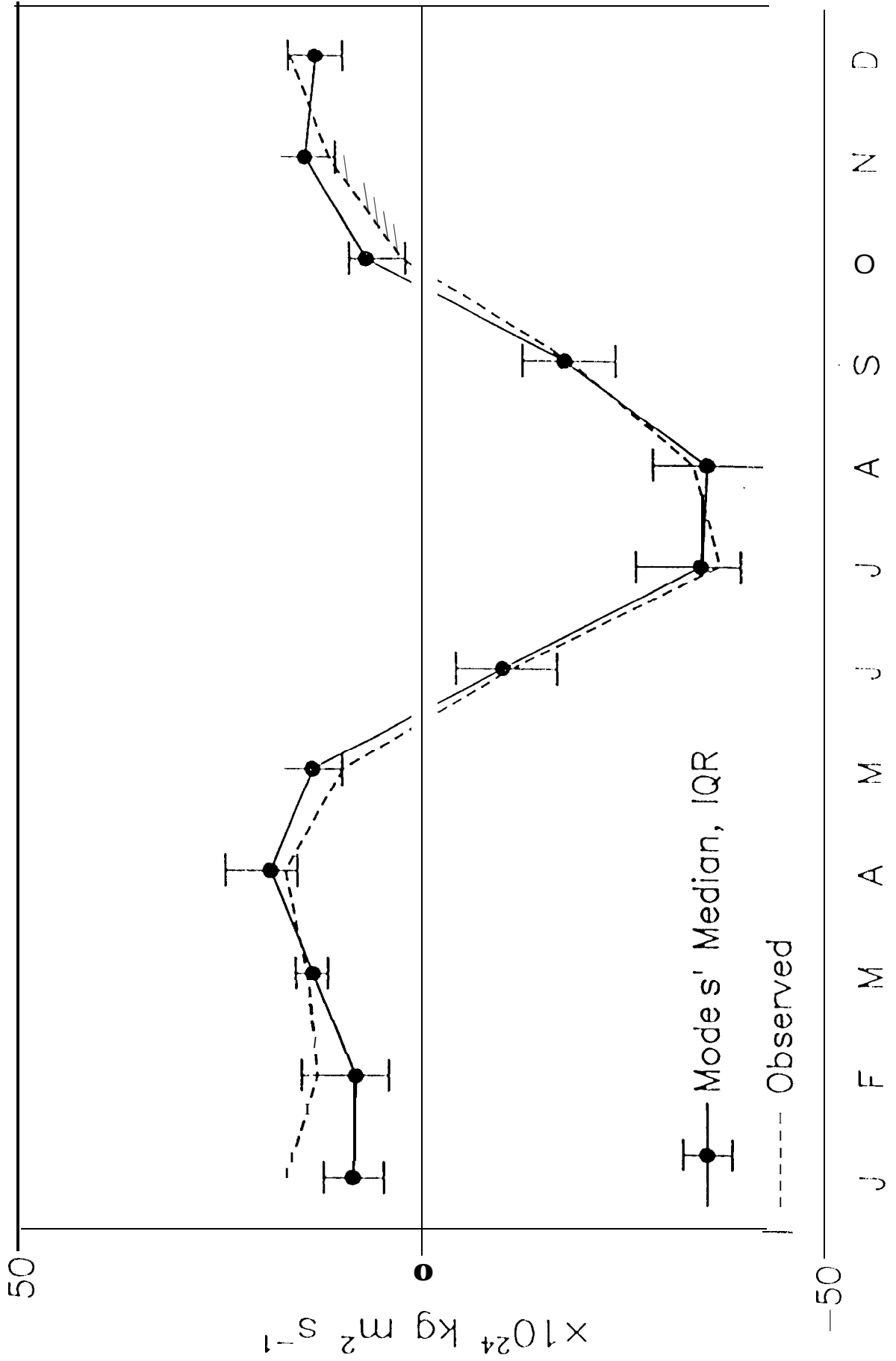
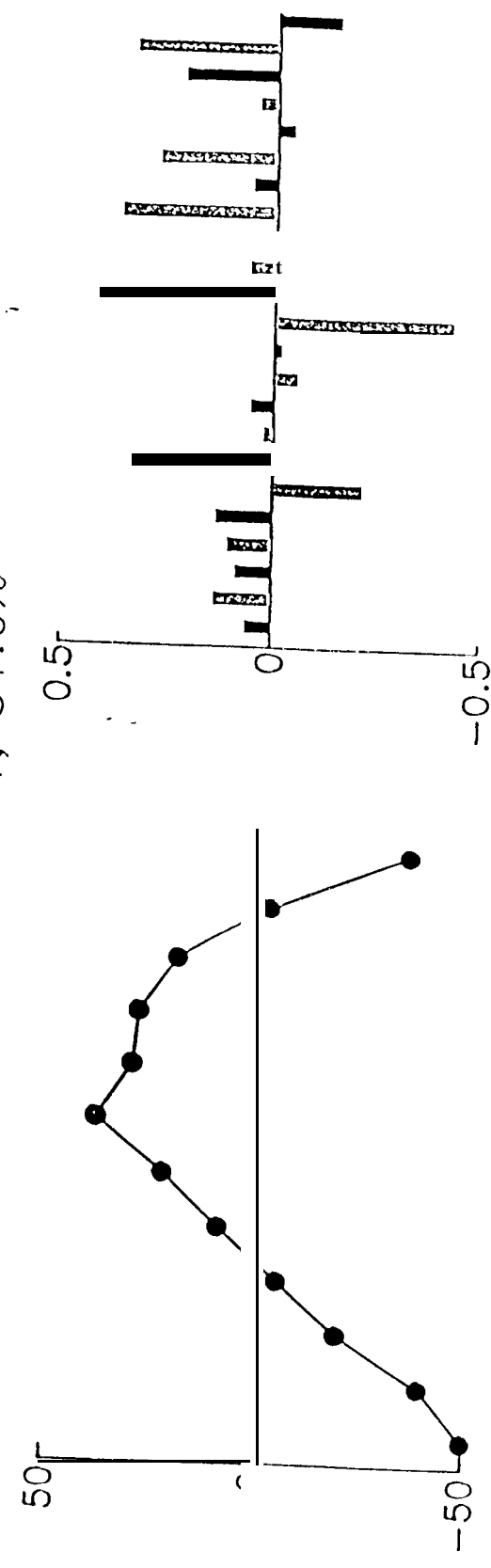


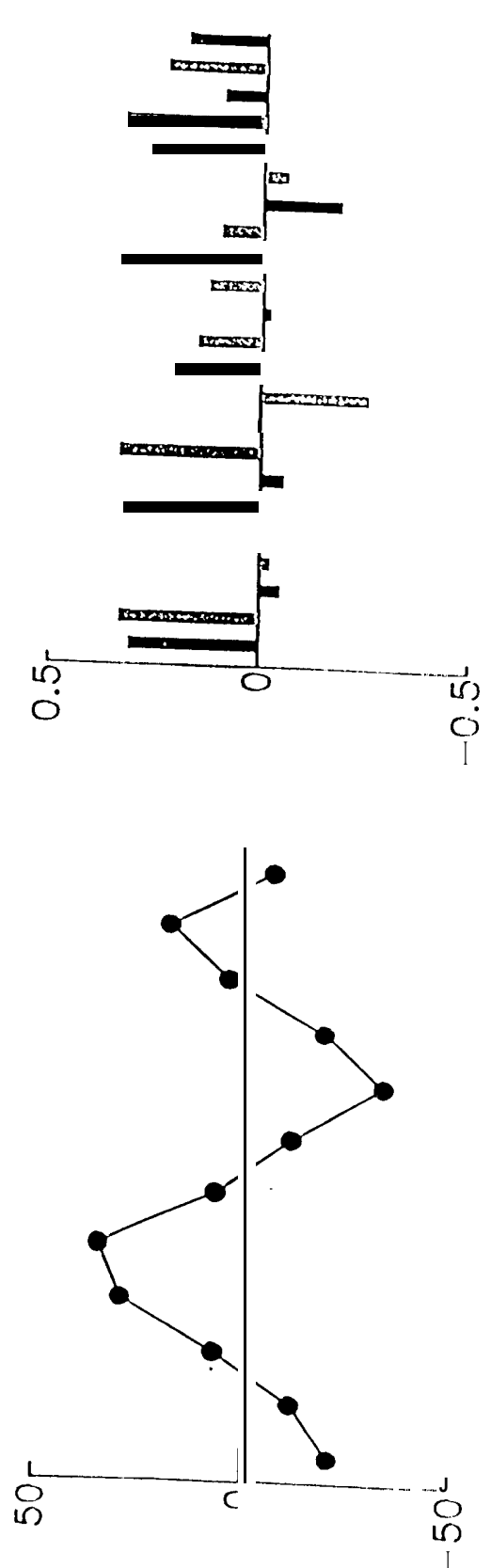
Figure 8

Seasonal errors EOF

EOF 1, 51.0%



EOF 2, 23.4%



Mode weights

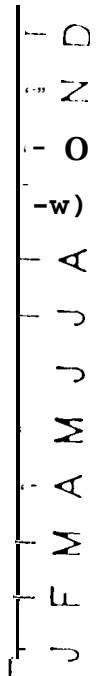
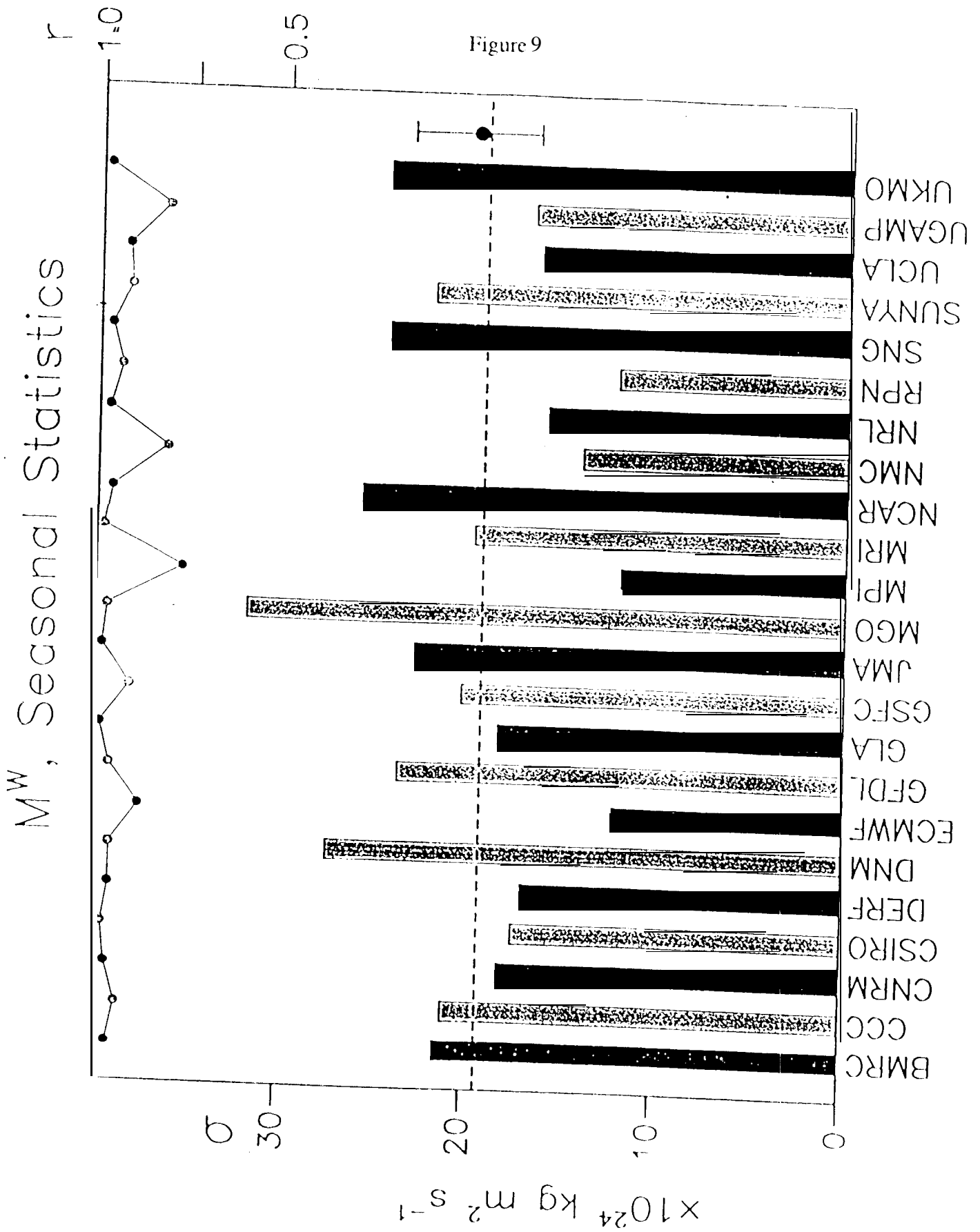


Figure 9



a. Observed Belt Momentum Variance, Seasonal

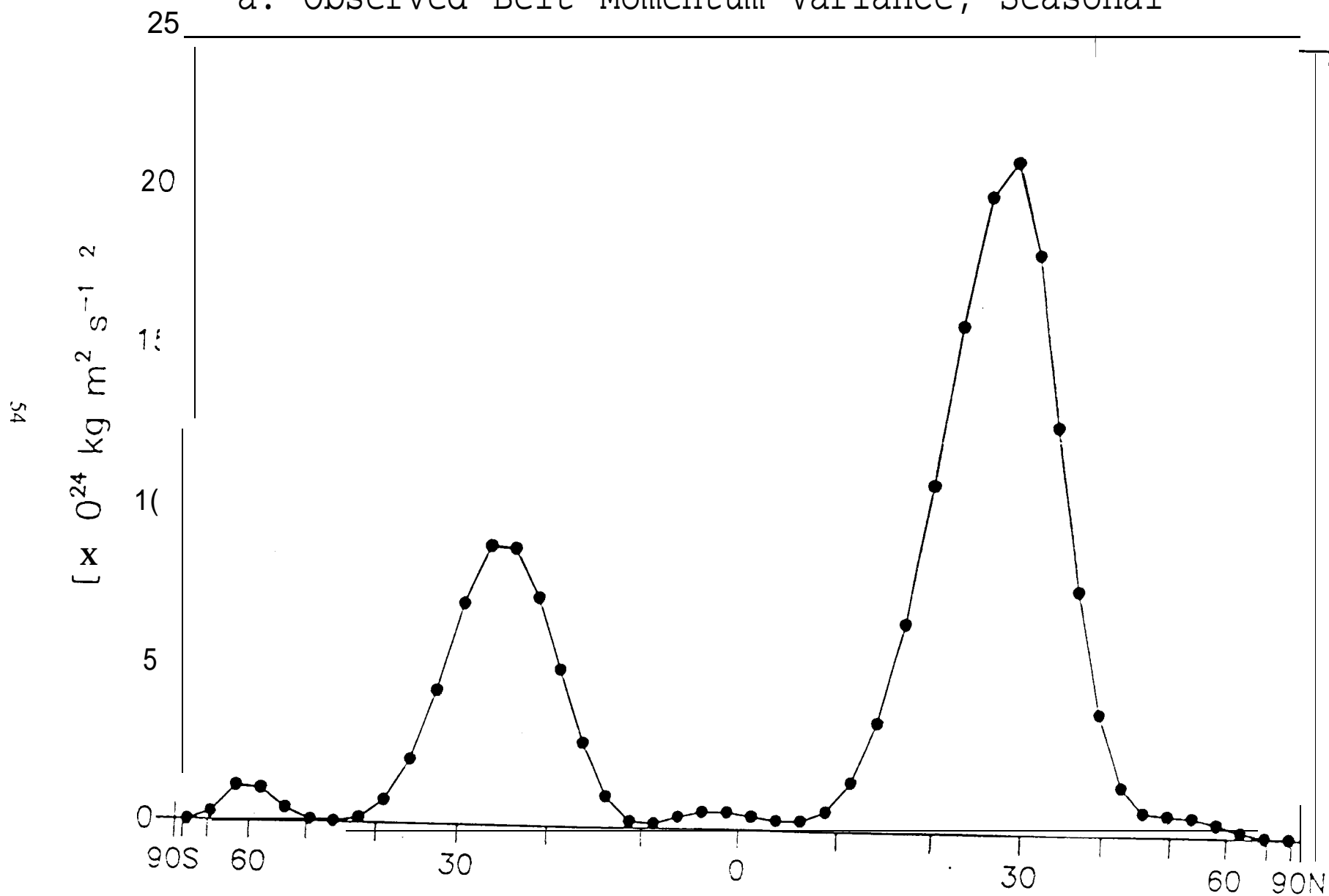
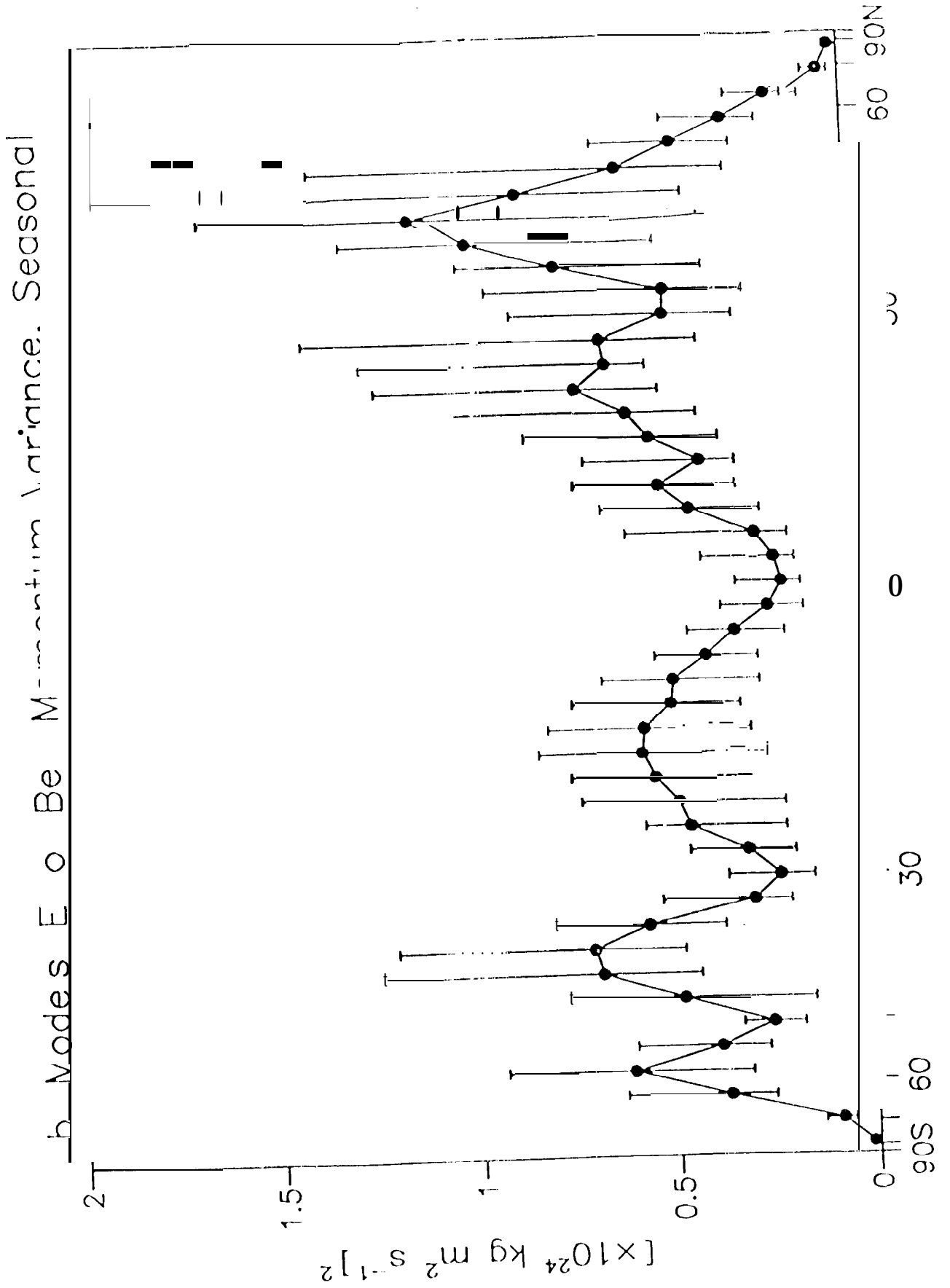


Figure 10a

Figure 10b



Seasonal Covariance with Global M^W Error, Seasonal

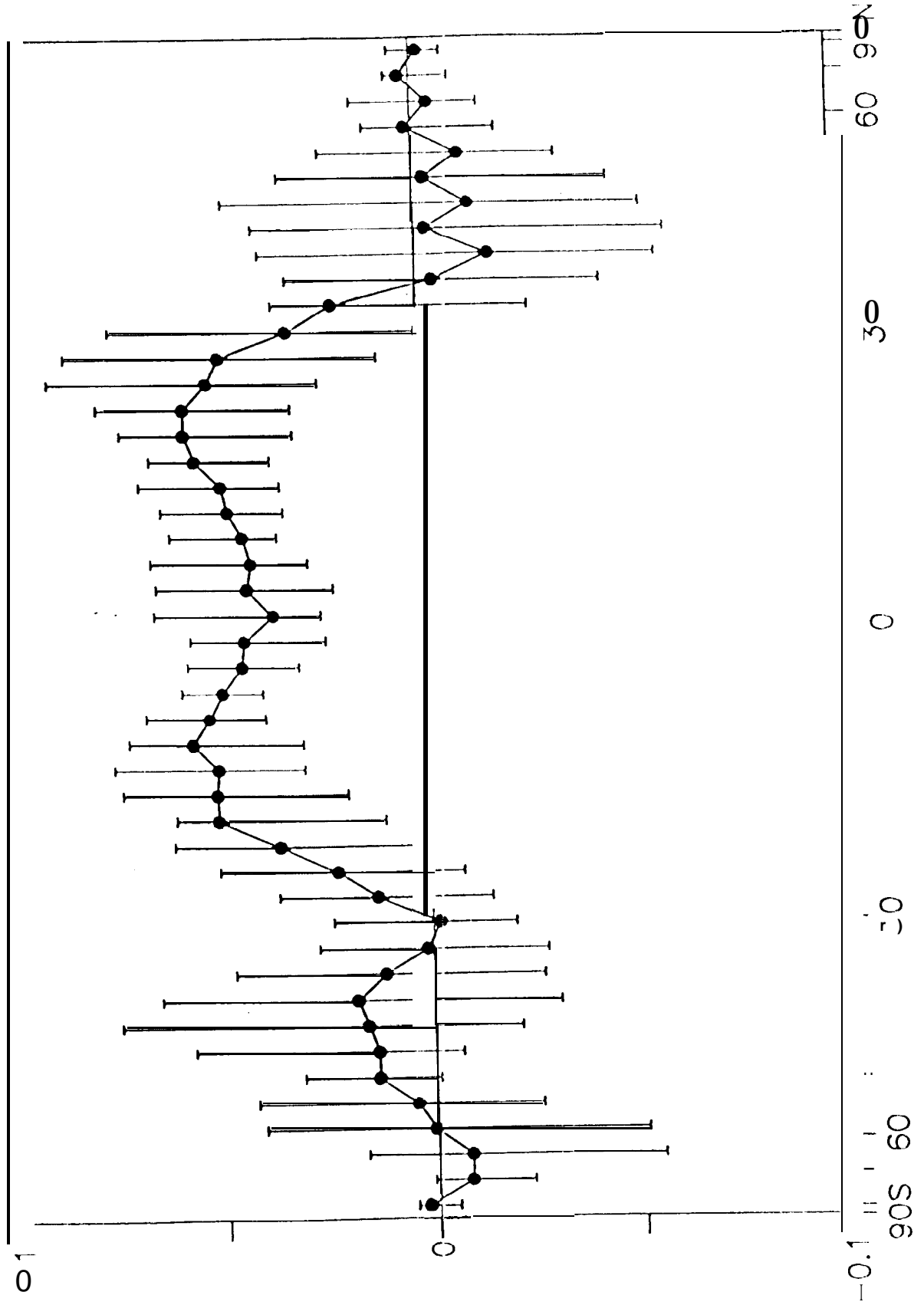


Figure 10c

Figure. 11

M^W , nterannus Component

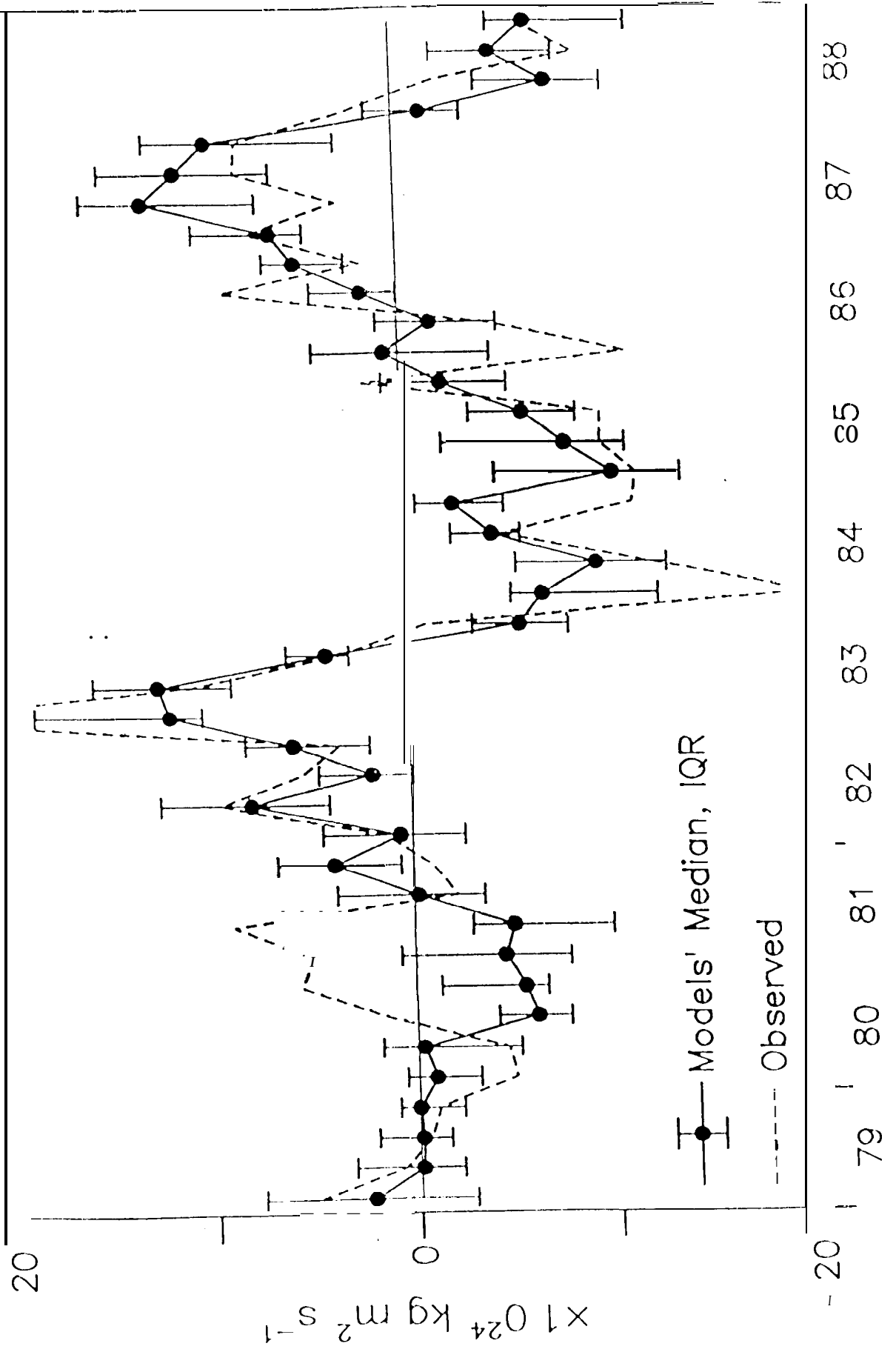


Figure 12

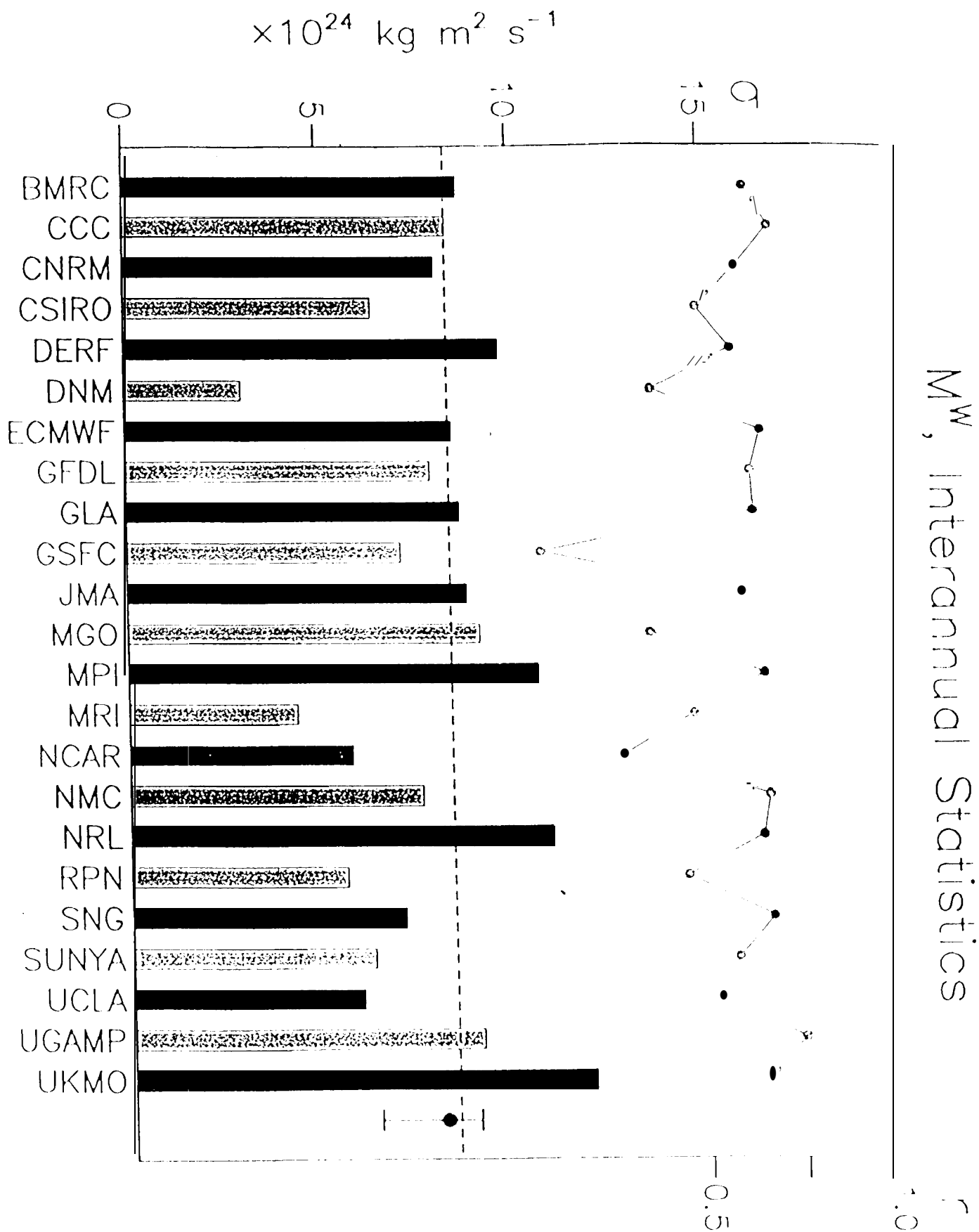


Figure 13a

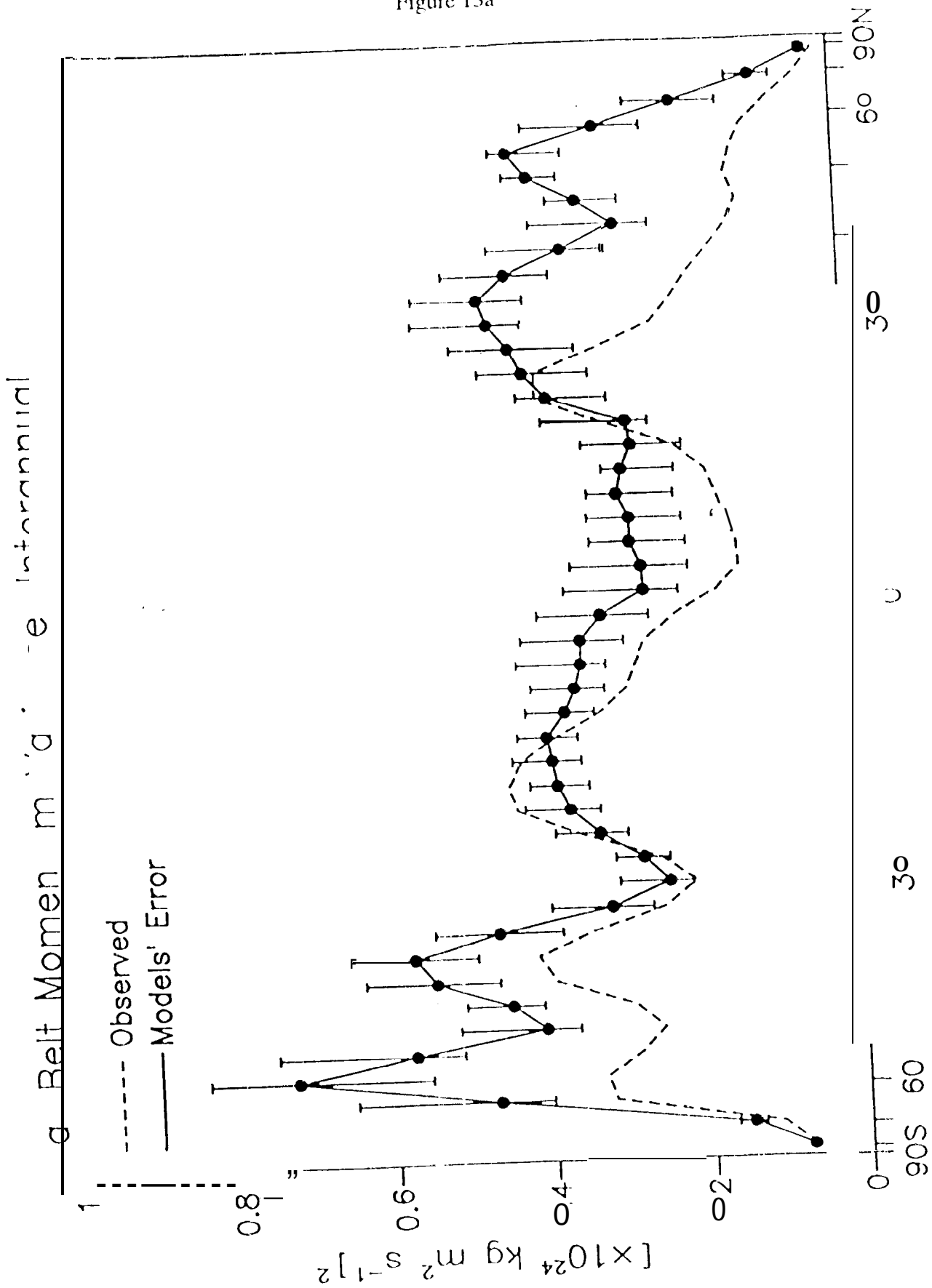


Figure 13b

